

The Sec14-like phosphatidylinositol transfer proteins Sec14I3/SEC14L2 act as GTPase proteins to mediate Wnt/Ca²⁺ signaling

Bo Gong, Weimin Shen, Wanghua Xiao, Yaping Meng, Anming Meng*, Shunji Jia*

State Key Laboratory of Membrane Biology, Tsinghua-Peking Center for Life Sciences, School of Life Sciences, Tsinghua University, Beijing, China

Abstract The non-canonical Wnt/Ca²⁺ signaling pathway plays important roles in embryonic development, tissue formation and diseases. However, it is unclear how the Wnt ligand-stimulated, G protein-coupled receptor Frizzled activates phospholipases for calcium release. Here, we report that the zebrafish/human phosphatidylinositol transfer protein Sec14I3/SEC14L2 act as GTPase proteins to transduce Wnt signals from Frizzled to phospholipase C (PLC). Depletion of *sec14I3* attenuates Wnt/Ca²⁺ responsive activity and causes convergent and extension (CE) defects in zebrafish embryos. Biochemical analyses in mammalian cells indicate that Sec14I3-GDP forms complex with Frizzled and Dishevelled; Wnt ligand binding of Frizzled induces translocation of Sec14I3 to the plasma membrane; and then Sec14I3-GTP binds to and activates phospholipase C δ 4a (Plc δ 4a); subsequently, Plc δ 4a initiates phosphatidylinositol-4,5-bisphosphate (PIP₂) signaling, ultimately stimulating calcium release. Furthermore, Plc δ 4a can act as a GTPase-activating protein to accelerate the hydrolysis of Sec14I3-bound GTP to GDP. Our data provide a new insight into GTPase protein-coupled Wnt/Ca²⁺ signaling transduction.

DOI: [10.7554/eLife.26362.001](https://doi.org/10.7554/eLife.26362.001)

*For correspondence: mengam@mail.tsinghua.edu.cn (AM); jiasj@mail.tsinghua.edu.cn (SJ)

Competing interests: The authors declare that no competing interests exist.

Funding: See page 20

Received: 27 February 2017

Accepted: 30 April 2017

Published: 02 May 2017

Reviewing editor: Hong Zhang, Institute of Biophysics, Chinese Academy of Sciences, China

© Copyright Gong et al. This article is distributed under the terms of the [Creative Commons Attribution License](https://creativecommons.org/licenses/by/4.0/), which permits unrestricted use and redistribution provided that the original author and source are credited.

Introduction

Wnt ligands, a large family of secreted lipoglycoproteins, control a large number of developmental events in animals, including cell fate, migration and polarity, embryonic patterning, organogenesis and stem cell renewal (*MacDonald et al., 2009; Clevers and Nusse, 2012*). Mammals express 19 Wnt members that bind to a corresponding receptor among 10 Frizzled (Fz) receptors (*Niehrs, 2012*). These receptors have a seven transmembrane span motif characteristic of G protein-coupled receptors, and, following binding of a Wnt ligand, activate different downstream pathways (*Semenov et al., 2007; Loh et al., 2016*). In the canonical Wnt pathway, Wnt signaling stabilizes cytoplasmic β -catenin and thereby promotes its nucleus translocation and accumulation to activate downstream target genes transcription (*MacDonald et al., 2009*). Wnts also signal through at least two β -catenin-independent (non-canonical) branches, the Wnt/Planar Cell Polarity (PCP) and Wnt/Ca²⁺ pathways, during vertebrate development. They are both devoted to modulate cytoskeleton organization to coordinate or polarize cell convergent and extension movements (*Veeman et al., 2003; Kühl et al., 2000b; Angers and Moon, 2009*). In the Wnt/PCP pathway, the monomeric small GTPases such as RhoA and Rac1 are required for transducing Wnt-Fz signaling to c-Jun N-terminal Kinase (JNK) to direct cell polarity and cell movement (*Huelsken and Birchmeier, 2001; Wodarz and Nusse, 1998*).

The Wnt/Ca²⁺ signaling pathway emerged with the observations that overexpression of *Xenopus* Wnt5A and rat Fz2 in zebrafish embryos stimulated intracellular calcium flux and calcium-activated

intracellular pathway (Kohn and Moon, 2005; Slusarski et al., 1997a, 1997b). It is demonstrated that pertussis toxin-sensitive heterotrimeric G protein subunits, e.g., $G_{\alpha o}$ and $G_{\alpha t}$, are required for transducing the specific Wnt-Fz-Dishevelled complex signals downstream to activate phospholipase C (PLC) (Halleskog et al., 2012; Halleskog and Schulte, 2013; Liu et al., 1999). The activated PLC cleaves PIP_2 , a membrane-bound inositol lipid, into diacylglycerol (DAG) and inositol 1,4,5-triphosphate ($InsP_3$). DAG stimulates protein kinase C (PKC) to induce ERK phosphorylation, while $InsP_3$ binds to its corresponding receptor on the ER membrane, opening calcium channels for Ca^{2+} release and increasing cytoplasmic Ca^{2+} ion levels (Kadamur and Ross, 2013). Besides regulating cytoskeleton organization, Wnt/ Ca^{2+} also can influence CE movements through modulating calcium-dependent cell adhesion or dynamics of calcium storage and release (Kühl et al., 2001; Slusarski and Pelegri, 2007; Tada and Heisenberg, 2012; Wallingford et al., 2002). However, until now the interplay between Fz and heterotrimeric G/GTPase proteins in the Wnt/ Ca^{2+} signaling pathway is very controversial (Oner et al., 2013; Schulte and Bryja, 2007). Therefore, it remains mysterious and debated about how to orchestrate the upstream Wnt/Fz stimulation with downstream PLC/ Ca^{2+} components.

In recent years, a number of Sec14-like proteins have been identified and characterized. It has been demonstrated that dysfunction of Sec14-like proteins would cause various human diseases, such as breast cancer, prostate cancer, ataxia, and retinal degeneration syndromes (Cockcroft, 2012). Sec14-like proteins belong to atypical class III phosphatidylinositol transfer proteins (PITPs) (Allen-Baume et al., 2002) and consist of the versatile Sec14 domain associated with a GTPase motif of uncertain biological function (Habermehl et al., 2005; Novoselov et al., 1996; Merkulova et al., 1999). PITPs can transfer phosphatidylinositol (PI) and phosphatidylcholine (PC) between membranes, exchanging PI for PC and vice versa, in order to maintain balanced membrane lipid levels upon consumption of phosphoinositides (Wiedemann and Cockcroft, 1998). Although it has been established that PITPs integrate the lipid metabolome with phosphoinositide signaling cascades intracellularly, only very few studies indicate that PITPs can respond to extracellular molecular cues to initiate intracellular signaling (Xie et al., 2005; Kauffmann-Zeh et al., 1995). So far, there is no evidence about the biological importance of the GTPase motif in the Sec14-like proteins, as well as the crosstalk between PITP family proteins and Wnt/ Ca^{2+} signaling.

In this study, we investigated the role of the zebrafish Sec14I3 in embryonic development and the molecular mechanism of its action. We demonstrate that genetic depletion of maternal *sec14I3* results in defects in embryonic convergent and extension (CE) movements by impairing Wnt/ Ca^{2+} signaling. Biochemical and genetic data indicate that Sec14I3 can transduce, via its intrinsic GTPase activity, Wnt-Fz signaling to activate phospholipase C.

Results

Depletion of maternal *sec14I3* impairs the gastrulation CE movements in zebrafish

We are interested in roles of maternal genes in early development of zebrafish embryos. Our previous RNA-seq data suggested that, among three SEC14-like phosphatidylinositol transfer protein genes (*sec14I1*, *sec14I2*, and *sec14I3*), *sec14I3* is highly expressed in zebrafish eggs. Whole mount in situ hybridization (WISH) confirmed the abundance of *sec14I3* transcripts during cleavage and early blastula stages (Figure 1A). Thereafter, *sec14I3* mRNA decreases to undetectable levels by the shield stage and increases again after the bud stage with enrichment in the vasculature cells (Figure 1A).

To study *sec14I3* function, we first used two antisense morpholino oligonucleotides (MO), *sec14I3*-MO1 and *sec14I3*-MO2, which targeted different sequences around the 5' untranslated region of *sec14I3* mRNA, to block its translation (Figure 1—figure supplement 1A). Since *sec14I3*-MO1 was more effective than *sec14I3*-MO2 (Figure 1—figure supplement 1B), *sec14I3*-MO1 was used in subsequent experiments. Compared to standard MO (std-MO)-injected embryos, embryos injected with *sec14I3*-MO1 displayed slower epiboly in a dose-dependent manner (Figure 1B).

To substantiate the knockdown effect, we generated four *sec14I3* mutant lines by targeting the sequence around the translation start codon using transcriptional activator-like effector nucleases (TALENs) technology (Figure 1—figure supplement 1C). The first line we obtained was *sec14I3^{tsu-}*

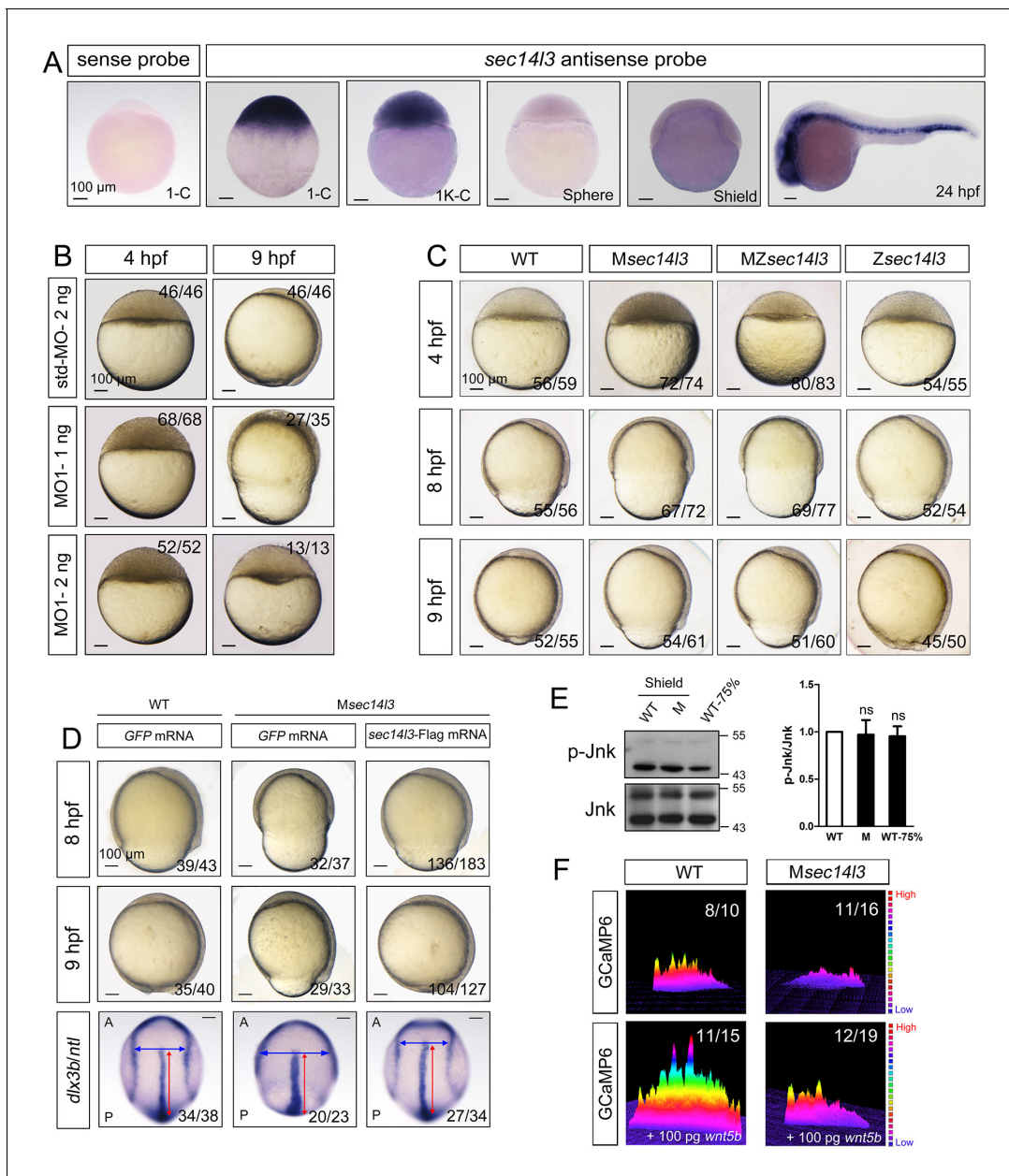


Figure 1. *Sec14l3* depletion impairs CE movements and Wnt/Ca²⁺ signaling in zebrafish. (A) Spatiotemporal expression pattern of *sec14l3*. Embryos were laterally viewed with animal pole to the top or with anterior to the left. Scale bars, 100 μ m. (B) Morphological defects in *sec14l3* morphants during gastrulation. Scale bars, 100 μ m. (C) Morphological defects in *Msec14l3*, *MZsec14l3* and *Zsec14l3* mutants. Scale bars, 100 μ m. (D) *sec14l3* mRNA rescue assay. 150 pg *sec14l3* mRNA was injected into *Msec14l3* mutants for rescue, and then the morphology and *dlx3b/ntl* marker gene expression were examined. First two panels: lateral views; last panel: dorsal views. Blue and red two-way arrows indicate the width of neural plate and the length of notochord respectively. Scale bars, 100 μ m. (E) Phosphorylation level of Jnk in *Msec14l3* mutant embryos. p-Jnk (Thr183/Tyr185) and total Jnk were examined at the shield (Morphology comparable) and 75% epiboly stage (Time point comparable) by western blot. Quantification of relative protein levels is shown on the right, represented by mean \pm SEM in three separate experiments (see also **Figure 1—source data 1**, ns, non-significant). (F) Differential induction of calcium transient activity in zebrafish embryos. Representative calcium release profiles of embryos at the sphere stage in wild-type and *Msec14l3* mutant background with or without *wnt5b* mRNA overexpression. The color bar represents the number of transients: red represents high numbers, blue represents lower numbers, and the peaks represent more active regions. In all panels, the ratio in the right corner indicated the number of embryos with altered phenotypes/the total number of observed embryos.

DOI: 10.7554/eLife.26362.002

The following source data and figure supplements are available for figure 1:

Source data 1. Numerical data for **Figure 1E**, **Figure 1—figure supplement 1D** and **Figure 1—figure supplement 2B**.

DOI: 10.7554/eLife.26362.003

Figure 1 continued on next page

Figure 1 continued

Figure supplement 1. Effectiveness of *sec14l3* MOs and generation of *sec14l3* mutants.

DOI: 10.7554/eLife.26362.004

Figure supplement 2. *Sec14l3* depletion has no effect on cell proliferation or cell cycle progression, as well as cell adhesion between envelop layer (EVL) and deep cells (DC).

DOI: 10.7554/eLife.26362.005

Figure supplement 3. *SEC14L2* depletion inhibits Wnt/ Ca^{2+} transduction in PC3 cells.

DOI: 10.7554/eLife.26362.006

td¹⁰, which carried a 10 bp deletion (−3 to +7). Some zygotic mutants (*Zsec14l3*) of this line survived to adulthood, allowing production of maternal (*Msec14l3*) and maternal-zygotic mutants (*MZsec14l3*). In two-cell stage *Msec14l3* or *MZsec14l3* embryos, *sec14l3* transcripts were almost eliminated (**Figure 1—figure supplement 1D**), which was likely due to unstable property of mutant mRNAs. Both *Msec14l3* and *MZsec14l3* mutant embryos showed a slower epibolic process, which mimicked *sec14l3* morphants, whereas *Zsec14l3* embryos appeared normal (**Figure 1C**). Therefore, the contribution of *sec14l3* to gastrulation cell movements is a strictly maternal-effect. Interestingly, this maternal effect lasted through larval stages as evidenced by a reduced body length in *Msec14l3* mutants compared with control embryos (**Figure 1—figure supplement 1E**). It appeared that cell proliferation and cell cycle progression in *Msec14l3* mutant embryos were unaffected, then we focused on the event of cell movements (**Figure 1—figure supplement 2A**). At the bud stage (about 10 hpf), *Msec14l3* mutant embryos had a broader and shorter embryonic axis, which was marked by the midline marker *ntl* and the neural plate border marker *dlx3b* (**Figure 1D**), indicative of impaired CE movements. Moreover, the defective CE movements of *Msec14l3* embryos were not caused by cell adhesion defects between envelop cell layer (EVL) and deep cells (**Figure 1—figure supplement 2B**) and could be rescued by *sec14l3* overexpression (**Figure 1D**). Maternal mutants of other *sec14l3* lines (*sec14l3^{tsu-td4}*, *sec14l3^{tsu-td8}* and *sec14l3^{tsu-td9}*), which were obtained later on, also exhibited similar phenotypes. Taken together, these data strongly suggest that the maternal, but not the zygotic, contribution of *sec14l3* is critical for normal epiboly and CE movements during gastrulation.

Sec14l3 is required for Wnt/ Ca^{2+} signaling transduction

Since both Wnt/PCP and Wnt/ Ca^{2+} can regulate cell movements during embryonic development (*Cha et al., 2008; Niehrs, 2012; Lin et al., 2010; Webb and Miller, 2003*), we then examined which pathway was affected in *sec14l3* mutant embryos. Results showed that Wnt/PCP signaling readout, the phosphorylated Jnk, p-Jnk(Thr183/Tyr185), was almost unaffected in *Msec14l3* mutant embryos, compared to wild-type embryos both at the same developmental stage and time point (**Figure 1E**). Human *SEC14L2*, rather than *SEC14L3*, is expressed in HEK293T and Wnt5-responsive PC3 cells, allowing easier examination of the effect of SEC14-like proteins on related signaling pathways (**Figure 1—figure supplement 3A**) (*Ye et al., 2004*). Like zebrafish *sec14l3*, knockdown of *SEC14L2* in PC3 cells had little effect on p-JNK expression levels (**Figure 1—figure supplement 3B and C**). Therefore, we speculate that *Sec14l3/SEC14L2* may not be crucial for the Wnt/PCP signaling pathway.

Next, we used the calcium indicator protein GCaMP6 to visualize calcium transients by confocal microscopy in zebrafish embryos, according to the method reported by Slusarski et al. (*Chen et al., 2013; Nakai et al., 2001; Slusarski et al., 1997a*). We found that the frequency of calcium release was attenuated obviously in *Msec14l3* mutant embryos either at the basal level or upon Wnt5b stimulation (**Figure 1F**). We therefore conclude that maternal *Sec14l3* plays a role in Wnt ligand-dependent calcium release during embryogenesis. Similarly, Wnt5a-induced calcium signal in PC3 cells was also decreased when *SEC14L2* was knocked down by shRNA (**Figure 1—figure supplement 3D**). Thus, *Sec14l3/SEC14L2* take part in Wnt/ Ca^{2+} signaling transduction by promoting intracellular calcium release.

Sec14l3 forms complexes with Fz, Dvl and PLC

Fz, Dishevelled (Dvl) proteins and PLC are all implicated in Wnt-induced calcium release (*Kühl et al., 2000a; Komiya and Habas, 2008*), but the underlying mechanisms remain elusive. We wondered

whether Sec14I3 could associate with these proteins and performed co-immunoprecipitation (Co-IP) in mammalian cells. We found that Sec14I3 associated with C-terminal of human Fz5 (hFz5-CT) and rat Fz2 (Rfz2-CT) in HEK293T cells (**Figure 2A**, **Figure 2—figure supplement 1A**). The *in vitro*-synthesized hFz5-CT and Rfz2-CT could be pulled down by GST-Sec14I3 (**Figure 2B**). These results support the idea that Sec14I3 directly interacts with Fz proteins. Our domain mapping analysis revealed that the N-terminal CARL-TRIO domain and the C-terminal GOLD domain of Sec14I3 were crucial for its interaction with Rfz2-CT (**Figure 2—figure supplement 1A–C**).

Then, we tested physical interaction of Sec14I3 with different Dvl proteins. Co-IP results revealed that Sec14I3 physically interacted with human DVL1, DVL2 or DVL3 in HEK293T cells (**Figure 2C**). Used as a representative, Myc-tagged mDvl2 was determined to directly interact with GST-Sec14I3 (**Figure 2D**). And in MCF7 cells, endogenous SEC14L2 interacted with DVL2 (**Figure 2E**). In addition, this interaction was further validated in zebrafish embryos by overexpressing xDvl2-Myc and Flag-Sec14I3 mRNAs (**Figure 2—figure supplement 1D**). Deletion analysis showed that the Sec14I3's Sec14 domain, but neither the CARL-TRIO nor GOLD domain, was essential for interaction with mDvl2 (**Figure 2—figure supplement 1A,B and E**). On the other hand, the DEP form of xDvl2, consisting of the DEP domain and the C-terminal region of xDvl2, was sufficient for the interaction with Sec14I3 (**Figure 2—figure supplement 1A and F**).

Next, we tested the physical interactions between zebrafish Sec14I3 and Plc δ family members, including Plc δ 1a, Plc δ 3b and Plc δ 4a that are essential for PIP₂ hydrolysis into DAG and InsP₃. As shown in **Figure 2F**, immunoprecipitation of Flag-tagged Sec14I3 in HEK293T cells retrieved HA-tagged Plc δ 4a and Plc δ 3b, but not Plc δ 1a. Furthermore, Plc δ 4a-HA and GST-Sec14I3 fusion proteins were expressed in *E. coli* and purified for pull down assay, which showed a direct interaction between them (**Figure 2G**). Additionally, we also found their interaction in zebrafish embryos (**Figure 2—figure supplement 1G**). Domain mapping analysis revealed that the CARL-TRIO domain and the GOLD domain of Sec14I3, unlike the Sec14 domain, were crucial for interaction with the N2 region of Plc δ 4a, including the PH and the EF hand domains (**Figure 2—figure supplement 1A,B,H and I**). Therefore, Sec14I3 utilizes different domains to interact with xDvl2 and Plc δ 4a.

To test whether Sec14I3, Fz and Dvl form a complex, we performed two-step Co-IP experiment. Results showed that hFz5-CT-Myc was present in the GST-Sec14I3-Dvl2-Flag complex (**Figure 2H**), suggesting the presence of the hFz5/Dvl2/Sec14I3 ternary complexes. Furthermore, we found that mDvl2 was present in the Plc δ 4a complexes, as well as in the Plc δ 3b complexes, but absent in the Plc δ 1a complexes (**Figure 2I**), which were similar to Sec14I3-Plc δ selective interactions (**Figure 2F**). DVL2 was also proved to interact with endogenous PLC δ 4a in MCF7 cells (**Figure 2E**). Moreover, we found that different Wnt ligands stimulation could result in distinct calcium responses. Among of them, Wnt5a had a strong capacity to promote calcium release in PC3 cells (**Figure 2—figure supplement 2A**, and [Thrasivoulou et al., 2013]). Upon Wnt5a stimulation, mDvl2-Plc δ 4a complex formation could be enhanced in PC3 cells, and knockdown of SEC14L2 led to a drastic reduction of mDvl2-Plc δ 4a complexes (**Figure 2J**), indicating the presence of the mDvl2/Sec14I3/Plc δ 4a ternary complexes.

Interestingly, Sec14I3-GFP could be co-immunoprecipitated with Sec14I3-Flag through its CARL-TRIO domain and GOLD domain (**Figure 2—figure supplement 2B and C**), suggesting oligomerization of Sec14I3. It is possible that Sec14-like protein oligomers may facilitate the formation of complexes with Fz, Dvl and Plc δ proteins.

Sec14I3 is required for PLC-catalyzed hydrolysis of PIP₂

Sec14-like proteins are members of PITP and assumed to transfer phosphoinositides (PIs) to the plasma membrane (PM) (Nile et al., 2010; Kearns et al., 1998; Wiedemann and Cockcroft, 1998; Wirtz, 1991). To test whether human SEC14L2 and zebrafish Sec14I3 have an effect on PI derivatives accumulation at the PM, we first measured levels of PIP₂ in HEK293T cells, the lipid substrate of PLC, using a PH probe, which consists of a GFP-tagged PH domain from PLC δ 1 that specifically binds to PIP₂ (Várnai and Balla, 1998; Idevall-Hagren and De Camilli, 2015). If the PI transfer activity of SEC14L2 is blocked, the PIP₂ level at the PM should be reduced. However, compared to control cells, transfection of PLC δ 1-PH-GFP DNA into HEK293T cells depleted of SEC14L2 resulted in more PLC δ 1-PH-GFP protein in the PM fraction (**Figure 3A**), indicative of more PIP₂ at the PM. Confocal imaging also revealed that the PLC δ 1-PH-GFP fluorescence at the PM was about 2-fold brighter in SEC14L2 shRNA stable cells than in the control cells (**Figure 3B**, top panel), which was

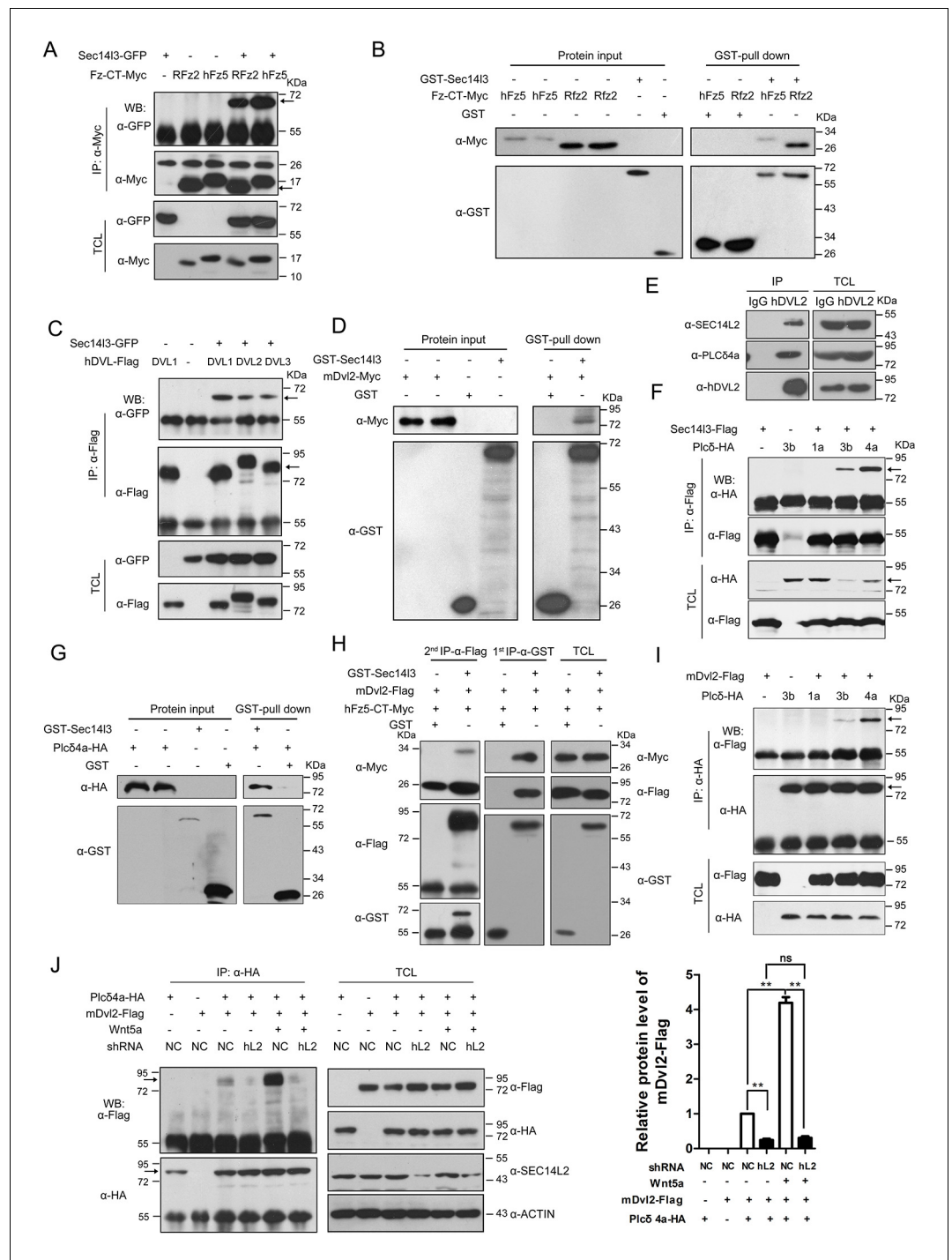


Figure 2. Sec14I3 orchestrates complex formation among Fz, Dvl and PLC. (A) Sec14I3 interacts with hFz2-CT and Rfz2-CT in HEK293T cells. IP, immunoprecipitation; WB, western blot; TCL, total cell lysates. The target protein in the precipitate was indicated by an arrow (same for other figures below). (B) Direct binding of Sec14I3 to hFz2-CT/Rfz2-CT *in vitro*. GST-Sec14I3 and hFz2-CT/Rfz2-CT-Myc were expressed in *E. coli* and purified. (C) Sec14I3 was detected in the protein complexes immunoprecipitated with Flag-tagged human DVL1/2/3 from HEK293T cells. (D) Direct binding of Sec14I3 to mDvl2 *in vitro*. GST-Sec14I3 and mDvl2-Myc were expressed in *E. coli* and purified. (E) Endogenous SEC14L2 and PLCδ4a interacts with DVL2 in MCF7 cells respectively. (F) Sec14I3 interacts with Plcδ3b and Plcδ4a in HEK293T cells. (G) Direct binding of Sec14I3 to PLCδ4a *in vitro*. GST-Sec14I3 and PLCδ4a-HA were expressed in *E. coli* and purified. (H) hFz5-CT, mDvl2 and Sec14I3 form a ternary complex *in vitro*. hFz5-CT-Myc and GST-Sec14I3 proteins purified from *E. coli* were incubated with mDvl2-Flag transfected cell

Figure 2 continued on next page

Figure 2 continued

lysates. The protein complexes were sequentially pulled down using GST (1 st IP- α -GST) and Flag antibody (2nd IP- α -Flag). Finally the second round immunoprecipitated proteins were detected using the corresponding antibodies. (I) mDvl2 interacts with Plc δ 3b and Plc δ 4a in HEK293T cells. (J) The interaction between mDvl2 and Plc δ 4a is restrained in the stable *SEC14L2* knockdown PC3 cells with or without 400 ng/ μ l Wnt5a stimulation. Quantification of relative mDvl2 levels from three independent experiments is shown as mean \pm SEM on the right (see also **Figure 2—source data 1**, ** $p < 0.01$; ns, non-significant).

DOI: [10.7554/eLife.26362.007](https://doi.org/10.7554/eLife.26362.007)

The following source data and figure supplements are available for figure 2:

Source data 1. Numerical data for relative protein level of mDvl2-Flag in **Figure 2I**.

DOI: [10.7554/eLife.26362.008](https://doi.org/10.7554/eLife.26362.008)

Figure supplement 1. Sec14I3 utilizes distinct domains to interact with Dvl2 and Plc δ 4a.

DOI: [10.7554/eLife.26362.009](https://doi.org/10.7554/eLife.26362.009)

Figure supplement 2. Sec14I3 can self-assemble into oligomers.

DOI: [10.7554/eLife.26362.010](https://doi.org/10.7554/eLife.26362.010)

consistent with changes of PIP₂ levels detected using a PIP₂ antibody (**Figure 3B**, lower panel). These results indicate that *SEC14L2* may be required for PIP₂ hydrolysis rather than for PIP₂ transfer.

Then, we switched to detect PIP₂ in zebrafish embryos by injecting *PLC δ 1-PH-GFP* mRNA. Compared to wild-type embryos, the *Msec14I3* mutant and *sec14I3* morphant embryos accumulated more PLC δ 1-PH-GFP/PIP₂ at the PM both at 4 and 6 hpf (**Figure 3C and F**, **Figure 3—figure supplement 1A and C**). With regard to PIP₃, the metabolic product of PIP₂, we also observed a similar PM elevation, indicated by AKT1-PH-mCherry probe, in *Msec14I3* mutants or morphants (**Figure 3—figure supplement 1B and C**). Therefore, consistent with *SEC14L2* in mammalian cells, depletion of *Sec14I3* leads to the PIP₂ accumulation at the PM likely due to inefficient activation of PLC but not deficiency of its PI transfer activity.

PLC-catalyzed hydrolysis of PIP₂ produces InsP₃ and DAG, two important secondary messengers in cell signaling transduction. InsP₃ signals release calcium from intracellular stores, while DAG induces PKC-mediated ERK phosphorylation (*Seitz et al., 2014*). In conjunction with measuring calcium levels (**Figure 1F**), we also measured phosphorylation of ERK (p-ERK) *in vitro* and *in vivo*. As expected, *SEC14L2* knockdown in HEK293T cells caused a reduction of p-ERK (Thr202/Tyr204), but had no effect on phosphorylated AKT (p-AKT Ser473) (**Figure 3—figure supplement 1D**). Similarly, both western blots and immunostaining of zebrafish embryos showed a significant decrease in p-Erk, but not p-Akt in *Msec14I3* mutants (**Figure 3—figure supplement 1E–G**). Collectively, these data establish a role for *Sec14I3* in regulation of PLC catalytic activity.

Wnt/Dvl-induced PLC activation is dependent on Sec14I3

To investigate whether *Sec14I3* mediates Wnt5b/Dvl2-induced PLC transduction *in vivo*, PIP₂ probe mRNA was injected into blastomeres at the 1 cell stage to visualize PIP₂, which was followed by injection of a cocktail of *wnt5b* and *GFP* mRNA into one cell at the 16–32 cell stage to produce mosaic expression of Wnt5b. While injection of *GFP* mRNA alone has no effect on the PIP₂ distribution (**Figure 3—figure supplement 2A and E**), PIP₂ at the PM in the region with ectopic Wnt5b was significantly reduced compared to in the region without ectopic Wnt5b in the same wild-type embryos (**Figure 3D**, upper panels and **Figure 3F**), suggesting that Wnt5b stimulates PLC-catalyzed PIP₂ hydrolysis. However, Wnt5b-dependent PLC activation was obviously inhibited in *Msec14I3* mutant embryos, as evidenced by a much minor reduction in the PIP₂ level (**Figure 3D**, lower panels and **Figure 3F**). Like *Sec14I3* depletion, *wnt5b* morphant embryos accumulated more PLC δ 1-PH-GFP/PIP₂ at the PM both at 4 and 6 hpf, compared to std-MO injected embryos (**Figure 3—figure supplement 2B and E**). More importantly, *wnt5b*-MO-induced PM accumulation of PLC δ 1-PH-GFP/PIP₂ and CE defects could be individually restored by mosaic and 1 cell stage injection of *sec14I3* mRNA (**Figure 3E,F** and **Figure 3—figure supplement 2C**). Taken together, these epistatic analyses indicate that *Sec14I3* can transduce Wnt5 signal to activate PLC in embryos.

Next, we used a truncated form of *Xenopus* Dishevelled, *xDsh-DelN*, to stimulate PLC-catalyzed PIP₂. *xDsh-DelN* is a N-terminal DIX domain deletion form that is sufficient to activate the Wnt/PCP and Wnt/Ca²⁺ but not Wnt/ β -catenin pathways (*Sheldahl et al., 2003*). As expected, *xDsh-DelN*

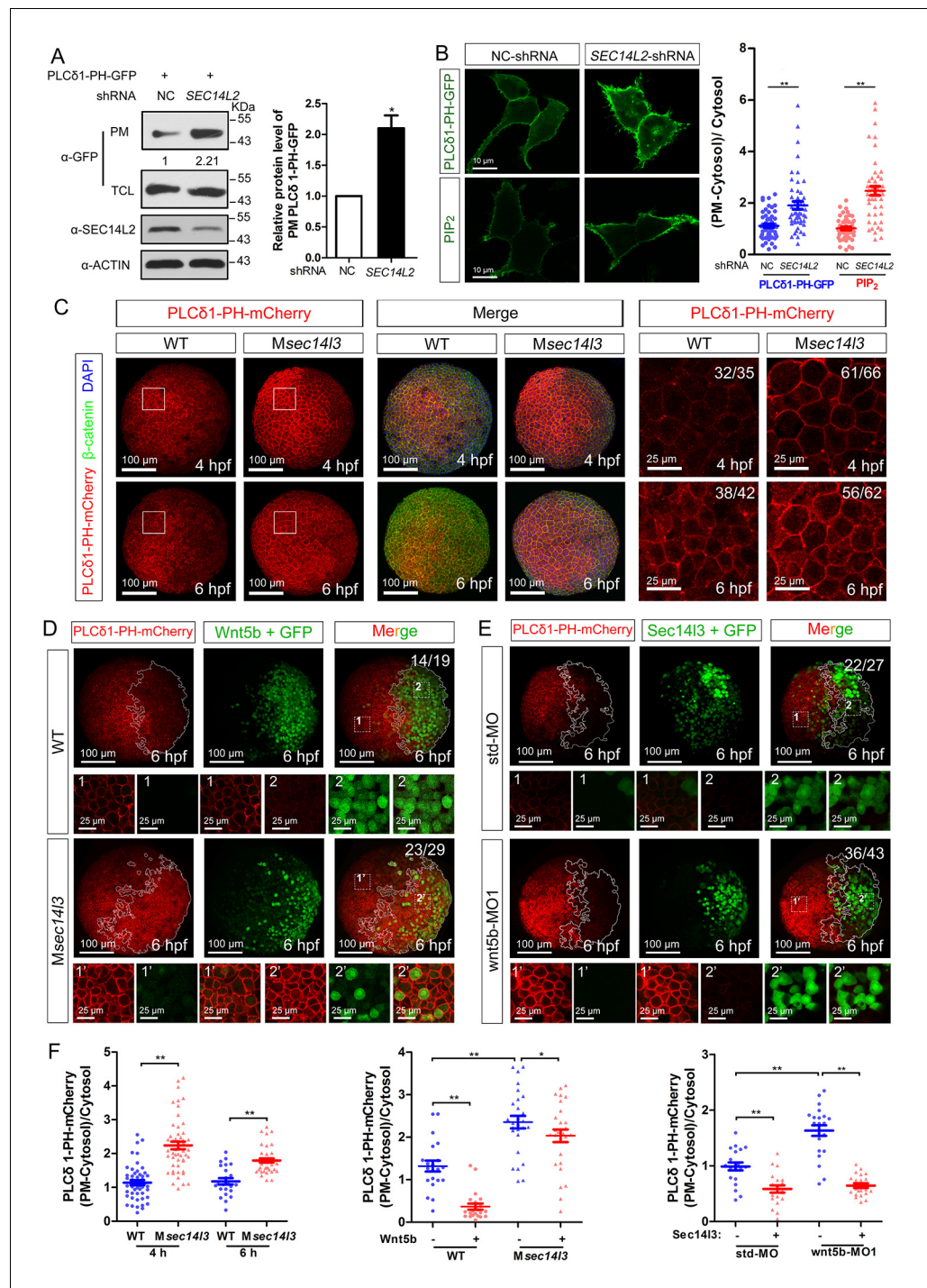


Figure 3. Sec1413 facilitates PLC-catalyzed PIP₂ hydrolysis induced by Wnt5b. (A) PM isolation analysis of PM PIP₂ levels using PLCδ1-PH-GFP as probe in HEK293T cells. Quantification data from three independent experiments are shown as mean ± SEM (see also **Figure 3—source data 1**, *p<0.05). (B) Immunofluorescence of PLCδ1-PH-GFP in first panel (transfected with PLCδ1-PH-GFP) and endogenous PIP₂ in second panel shows PIP₂ accumulation in the PM of stable SEC14L2-knockdown HEK293T cells. Data are presented as mean ± SEM (see also **Figure 3—source data 1**, **p<0.01; n ≥ 50 cells from three separate experiments). Scale bar, 10 μm. (C) Immunofluorescence of PLCδ1-PH-mCherry (red, PIP₂ probe), β-catenin (green, PM marker) and DAPI (blue, nucleus marker) shows PIP₂ accumulation in the PM of Msec14/3 mutant cells. The first two whole embryo panels are 3D views of z-stacks (n = 30 for 4 hpf, n = 34 for 6 hpf), while the last panel is enlarged views of single z-stack pictures (z = 8 for 4 hpf, z = 7 for 6 hpf) from regions encompassed by white boxes. Scale bars, 100 μm for whole **Figure 3 continued on next page**

Figure 3 continued

embryos; 25 μm for the enlarged columns. (D) Sec14I3 depletion compromises Wnt5b-induced degradation of PM PIP₂. Immunofluorescence of PLC δ 1-PH-mCherry (red) and GFP (green, indicating Wnt5b-expressed cells) is shown. Mosaic expression of 100 pg *wnt5b* mRNA was created in embryos with even distribution of PLC δ 1-PH-mCherry mRNA. White polygons outline GFP expressed cells and single z-stack pictures ($z = 10$) from numbered regions in the whole embryo panels (3D view of z-stacks) are enlarged. Scale bars, 100 μm for whole embryos; 25 μm for the enlarged panels. (E) *sec14I3* overexpression inhibits accumulation of PIP₂ in *wnt5b* morphant embryos. Mosaic expression of *sec14I3* by injecting 150 pg mRNA was created in embryos with even distribution of PLC δ 1-PH-mCherry mRNA in std-MO or *wnt5b*-MO injected embryos. Single z-stack pictures ($z = 11$) from numbered regions in the whole embryo panels (3D view of z-stacks) are enlarged. (F) PM PIP₂ quantification of (C–E) by calculating intensity of (PM-Cytosol)/Cytosol PLC δ 1-PH-mCherry. Data are shown as mean \pm SEM. (see also **Figure 3—source data 1**, ** $p < 0.01$; * $p < 0.05$; ns, non-significant; $n \geq 50$ cells from 10 embryos in three independent experiments).

DOI: [10.7554/eLife.26362.011](https://doi.org/10.7554/eLife.26362.011)

The following source data and figure supplements are available for figure 3:

Source data 1. Numerical data for **Figure 3A,B,F** and **Figure 3—figure supplements 1C–E** and **2E**.

DOI: [10.7554/eLife.26362.012](https://doi.org/10.7554/eLife.26362.012)

Figure supplement 1. *sec14I3* depletion results in PIP₂ and PIP₃ accumulation in the PM.

DOI: [10.7554/eLife.26362.013](https://doi.org/10.7554/eLife.26362.013)

Figure supplement 2. *wnt5b*-MO induced phenotypes can be restored by *sec14I3* mRNA.

DOI: [10.7554/eLife.26362.014](https://doi.org/10.7554/eLife.26362.014)

mosaic overexpression also lowered PIP₂ levels at the PM in injected clonal region of wild-type embryos (**Figure 3—figure supplement 2D**, upper panels and **2E**), while the *xDsh-DeIN-* dependent PLC activation was also inhibited in *Msec14I3* mutant embryos (**Figure 3—figure supplement 2D**, lower panels and **Figure 3—figure supplement 2E**). Therefore, it is speculated that Sec14I3 might mediate PLC activation downstream of Wnt5b/Dvl2 stimulation.

The GOLD and the G α domains of Sec14I3 are crucial for activating Plc δ activity

To determine which Sec14I3 domain(s) is/are critical for PLC activation, several truncated forms of Sec14I3 were combined with a PIP₂ probe for transfection in HEK293T cells. PM isolation assays showed that the truncated forms of CARL-TRIO domain (ΔN) and Sec14 domain (ΔS) still acted similarly to full-length Sec14I3, where a reduction was observed in the amount of PIP₂ at the PM (**Figure 4A**). However, rather than leading to PIP₂ degradation, forms of Sec14I3 lacking the GOLD domain (ΔG) or G α subunit ($\Delta\text{G}\alpha$) induced PIP₂ accumulation at the PM, suggesting that these forms are functioning as dominant negatives (**Figure 4A**). Similar results were observed with immunostaining (**Figure 4B**). To further evaluate this phenotype, we overexpressed the truncated forms of Sec14I3 in human *SEC14L2* knockdown stable cells, and found that enrichment of PIP₂ in the PM due to *SEC14L2* depletion was partially compromised by transfecting the full-length form of zebrafish Sec14I3, but not ΔG or $\Delta\text{G}\alpha$ forms (**Figure 4C**).

In consistent with the above biochemical data, overexpression of ΔG or $\Delta\text{G}\alpha$ mRNA in wild-type embryos led to a broader and shorter embryonic axis. And, neither the morphological epiboly defects nor marker gene-labeled CE defects seen in *Msec14I3* mutant embryos were rescued by either of these two truncated mRNAs (**Figure 4D**). Moreover, we found that ΔG or $\Delta\text{G}\alpha$ form overexpression caused a significant reduction of p-Erk in wild-type embryos (**Figure 4—figure supplement 1A and B**) and a much lower calcium responsiveness in PC3 cells (**Figure 4E and F**, **Figure 4—figure supplement 1C**), which were quite similar to what happened in *sec14I3* deficient situation (**Figure 1F**). Taken together, these data strongly suggest that the GOLD domain and the G α subunit domain of Sec14I3 are required for activating Plc δ activity.

Sec14I3 promotes PM translocation and hydrolytic activity of Plc δ 4a in response to Wnt5a stimulation

To further study the mechanism by which Sec14I3-mediated Wnt/PLC activation, we determined whether Sec14I3 translocated to the plasma membrane upon Wnt stimulation. As shown in

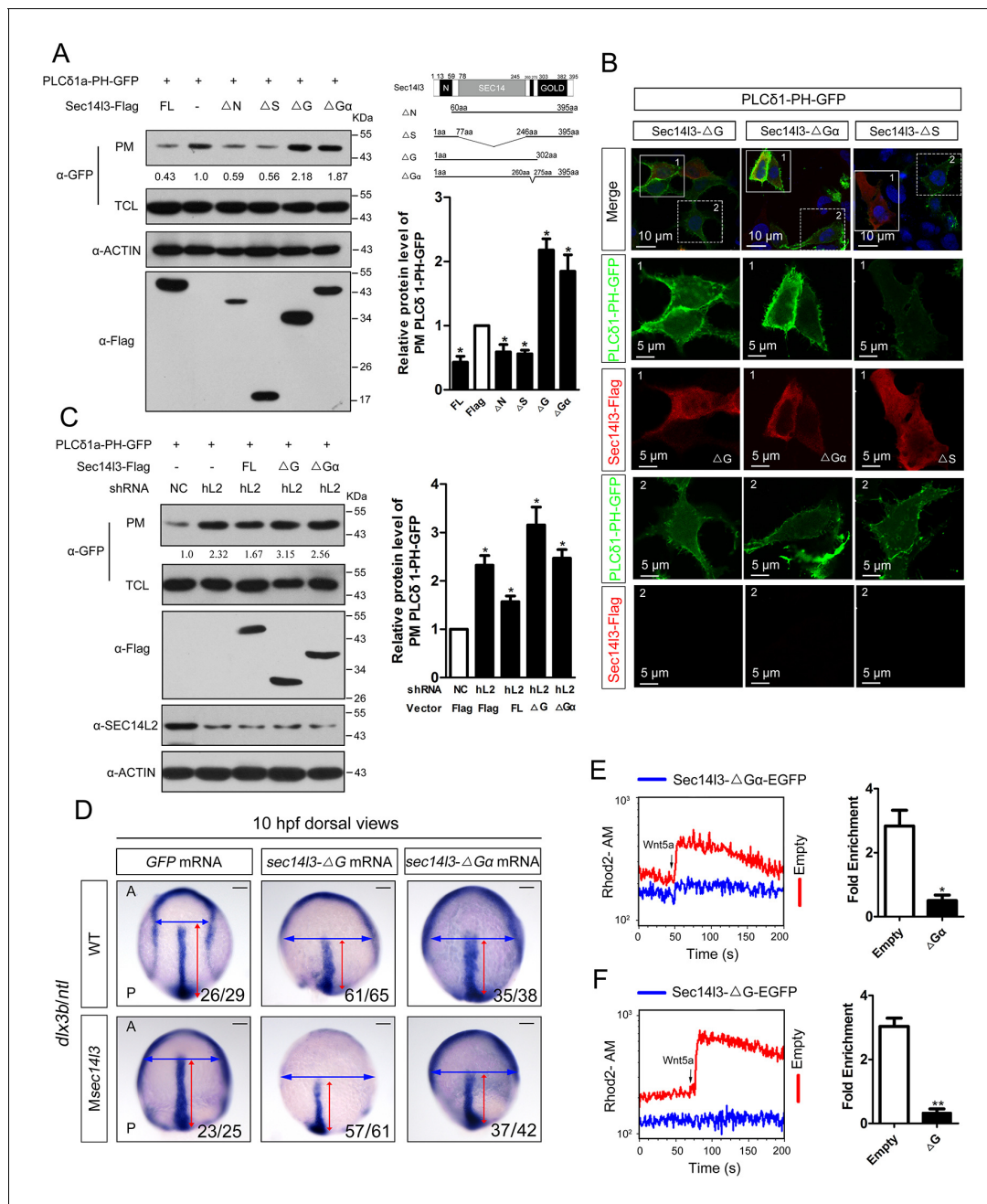


Figure 4. Sec14/3 activates PLC dependent on its GOLD and Gα domains. (A) Analysis of PIP₂ levels in the membrane. Different forms of Sec14/3 (right corner) were co-transfected with PLCδ1-PH-GFP into HEK293T cells, and PIP₂-bound PLCδ1-PH-GFP in the PM was detected by Western blot. The relative levels of PLCδ1-PH-GFP in the PM were quantified and presented as mean ± SEM from three independent experiments on the right (*p<0.05). (B) Immunofluorescence of PLCδ1-PH-GFP (green, PIP₂ probe) in HEK293T transfected with Sec14/3-ΔG, Sec14/3-ΔGα or Sec14/3-ΔS (red) respectively. Regions in white box are enlarged. Scale bar, 10 μm for the first panel and 5 μm for the enlarged panels. (C) PIP₂ accumulation in stable SEC14L2-knockdown cells was not abolished by overexpression of Sec14/3-ΔG or Sec14/3-ΔGα. Statistical data from three independent experiments are presented as mean ± SEM on the right (*p<0.05). (D) CE defects in embryos with ΔG and ΔGα Sec14/3 overexpression. *dlx3b/ntl* marker gene expression were examined at 10 hpf after *sec14/3-ΔG* and *sec14/3-ΔGα* mRNA injection respectively. Scale bar, 100 μm. (E–F) Flow cytometry of Wnt5a-induced calcium signals in PC3 cells transfected with Sec14/3-ΔGα or Sec14/3-ΔG (blue curves). Left panel shows the kinetic calcium influx over a time course. Right panel shows fold enrichment of calcium influx after Wnt5a stimulation. Data from three independent experiments are presented as mean ± SEM (*p<0.05, **p<0.01). Blue and red curves indicate the transfected and control group respectively. All numerical data represented as a graph in the figure are shown in **Figure 4—source data 1**. DOI: 10.7554/eLife.26362.015

The following source data and figure supplement are available for figure 4:

Figure 4 continued on next page

Figure 4 continued

Source data 1. Numerical data for relative protein level of PLC δ 1-PH-GFP or phosphorylation level ratio in **Figure 4** and **Figure 4—figure supplement 1**.

DOI: [10.7554/eLife.26362.016](https://doi.org/10.7554/eLife.26362.016)

Figure supplement 1. Δ G or Δ G α form overexpression caused a significant reduction of p-Erk in zebrafish embryos.

DOI: [10.7554/eLife.26362.017](https://doi.org/10.7554/eLife.26362.017)

Figure 5A, Figure 5—figure supplement 1A, Wnt5a stimulation induced a rapid translocation of Sec14I3-GFP to the PM, which was similar to the calcium sensor protein STIM1 (Liou et al., 2005) and enhanced by co-transfection of Dvl2. To rule out the possibility that Wnt5a-induced Sec14I3 PM recruitment might be a mere consequence of the calcium release, we tested the effect of hFz5/mDvl2 stimulation on Sec14 protein location in HEK293T and MCF7 cells that do not respond to hFz5/mDvl2 for calcium release (Mikels and Nusse, 2006; Foldynová-Trantírková et al., 2010). In HEK293T cells, endogenous SEC14L2 protein was enriched in the PM by hFz5 transfection, which was further enhanced by hFz5/mDvl2 coexpression (Figure 5B). Similar phenomenon was observed in MCF7 cells (Figure 5—figure supplement 1B). Additionally, we demonstrated that SEC14L2 knockdown had no effect on hFz5-mDvl2 interaction (Figure 5—figure supplement 1C), which suggests Fz-Dvl interaction might be independent of Sec14-like proteins. Therefore, combining the above data with pairwise biochemical interactions among Sec14I3, Fz and Dvl (Figure 2, Figure 2—figure supplement 1), we propose that Sec14I3 is a component of the Fz/Dvl/Sec14I3 complex, and its PM recruitment is promoted directly by Fz/Dvl in response to Wnt signaling stimulation.

Then we hoped to know how Sec14I3 regulates PLC activity. PLC has been proposed to serve as a membrane attachment enzyme, which hydrolyzes many substrates such as PIP₂ without dissociating from the lipid surface (Rhee, 2001). Therefore, we speculated that Sec14I3 might be necessary for recruitment of Plc δ 4a to the PM for executing function. To test this hypothesis, we analyzed the subcellular localization of Plc δ 4a upon overexpression of Sec14I3. Immunostaining results in MCF7 cells showed that Sec14I3 actually promoted the PM localization of Plc δ 4a after co-transfection with hFz5 and mDvl2 (Figure 5C). To determine which Sec14I3 domain(s) is/are critical for PLC recruitment, PM isolation assay was performed. In contrast to the cytoplasmic enrichment of Plc δ 4a in rest cells, there was a substantial enrichment of Plc δ 4a in the PM upon transfection with hFz5 or Rfz2 or both, which was enhanced by co-transfection with Δ G α or Δ G forms of Sec14I3, but not with Δ NG form (Figure 5D, Figure 5—figure supplement 1D). Furthermore, we found that Rfz2-induced enrichment of Plc δ 4a at the PM was inhibited in SEC14L2 knockdown cells, which could be restored by overexpressing the full-length, Δ G α or Δ G form, but not Δ NG form, of Sec14I3 (Figure 5E). Therefore, we speculate that both the TRIO-CARL domain and GOLD domain are required for recruiting Plc δ 4a to the PM upon Wnt receptors stimulation. Particularly, different from the receptors stimulation, Δ G form is sufficient to block Wnt5a-induced Plc δ 4a PM recruitment in PC3 cells, indicating a more important function of the C-terminal GOLD domain of the protein (Figure 5F), which is consistent with the functional analysis of PIP₂ localization (Figure 4A). Taken together, although Wnt5a ligand and its Fz receptors trigger Dvl2/Sec14I3-dependent Plc δ 4a PM recruitment in a slightly different way, possibly due to the diverse functions of the C-terminal GOLD2 domain upon ligand stimulation, Sec14I3 is important for the PM translocation of Plc δ 4a, which is mainly mediated by the C-terminal GOLD domain rather than the G α subunit domain.

The next question is whether Sec14-like protein-mediated PM translocation promotes Plc δ 4a binding to PIP₂. To address this issue, we performed liposome binding assay. As shown in Figure 5G, interaction between purified Plc δ 4a protein and liposome-bound PIP₂ was detected following incubation with HEK293T control cell lysate; however, this interaction was significantly weakened when the SEC14L2 knockdown cell lysate was used. This result indicates that Plc δ 4a accesses PIP₂ in a Sec14I3-dependent manner.

Sec14I3 functions as a GTPase protein in Wnt/PLC activation

We noticed that, although Sec14I3- Δ G α acts as a dominant negative form (Figure 4A–C), it works differently with Δ NG or Δ G form in mechanism, based on Plc δ 4a PM recruitment results (Figure 5D–F, Figure 5—figure supplement 1D). As previously reported, human SEC14-like proteins contain a proposed G α subunit and possess considerable GTPase activity (Habermehl et al., 2005; Novoselov et al., 1996; Merkulova et al., 1999; Novoselov et al., 1994). We wondered whether

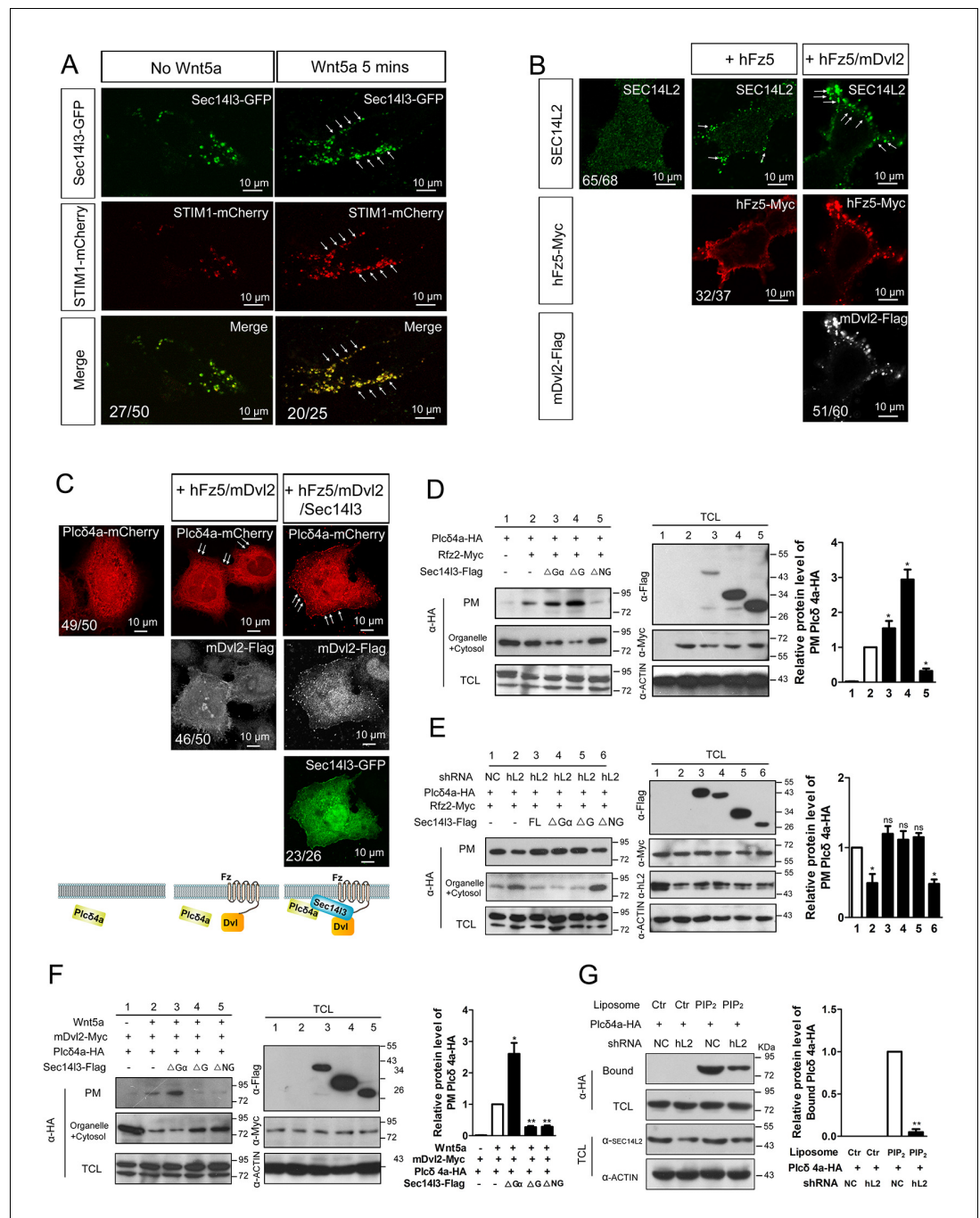


Figure 5. PM zone enriched-Sec1413 recruits PLC for activation upon Wnt5/Fz stimulation. (A) Co-localization of Sec1413 (green) with STIM1 proteins (red) in PC3 cells with or without Wnt5a stimulation. Arrows indicates PM-localized protein after Wnt5a stimulation. Scale bar, 10 μ m. (B) Immunofluorescence of endogenous SEC14L2 in HEK293T cells with or without hFz5/mDvl2 transfection. Arrows indicates PM-localized SEC14L2 (green). Scale bar, 10 μ m. (C) Immunofluorescence of Plc δ 4a-mCherry (red), mDvl2-Flag (gray) and Sec1413-GFP (green) in MCF7 cells. PM-localized Plc δ 4a (red) are indicated by arrows. The bottom panel show the schematic representation of transfected constructs in corresponding rows and an interpretation of the results. Scale bar, 10 μ m. (D) The Sec1413 CARL-TRIO and GOLD domains are important for Rfz2 mediated Plc δ 4a recruitment to the PM in the HEK293T cells. Statistical data from three independent experiments are presented as mean \pm SEM on the right (* p <0.05; ns, non-significant; same for other statistical data below). (E) Rfz2-mediated Plc δ 4a PM recruitment is abolished in stable SEC14L2-knockdown HEK293T cells and failed to be restored by Sec1413- Δ NG overexpression. Statistical data are presented. (F) The Sec1413 GOLD domain is important for Wnt5a mediated Plc δ 4a recruitment

Figure 5 continued on next page

Figure 5 continued

to the PM in PC3 cells. Statistical data are presented. (G) SEC14L2 depletion perturbs Plc δ 4a access to PIP₂. Equal amounts of purified Plc δ 4a protein and liposomes with or without PIP₂ were incubated with control or SEC14L2 depleted cell lysates. Statistical data are presented. All numerical data represented as a graph in the figure are shown in **Figure 5—source data 1**.

DOI: [10.7554/eLife.26362.018](https://doi.org/10.7554/eLife.26362.018)

The following source data and figure supplement are available for figure 5:

Source data 1. Numerical data for graphs in **Figure 5** and **Figure 5—figure supplement 1**.

DOI: [10.7554/eLife.26362.019](https://doi.org/10.7554/eLife.26362.019)

Figure supplement 1. The subcellular localization of Sec14I3 and its function in the Plc δ 4a PM recruitment.

DOI: [10.7554/eLife.26362.020](https://doi.org/10.7554/eLife.26362.020)

zebrafish Sec14I3 has the same property. The high sequence homology in the GTP binding motif and P loop region between zebrafish Sec14I3 and human SEC14L2/SEC14L3/SEC14L4 (**Figure 6A**) suggests a GTPase activity of zebrafish Sec14I3. Then we adopted BODIPY-FL-GTP γ S conventional assay and MESG-based single-turnover assay to detect the GTP binding and GTP hydrolysis activities of Sec14I3 (*Lin et al., 2014; McEwen et al., 2001; Töntson et al., 2012; Webb, 1992*). It estimated the K_{diss} and K_{hydr} rate constants for Sec14I3 to be $0.298 \pm 0.089 \text{ min}^{-1}$ and $0.151 \pm 0.025 \text{ min}^{-1}$ respectively (**Figure 6B–C**). These results indicated that Sec14I3 is a genuine GTPase protein with GTP binding and hydrolysis activities.

A hallmark of G proteins is their ability to undergo conformational switches, from the GDP-bound ‘off’ state to the GTP-bound ‘on’ state and vice versa (*Flock et al., 2015; Vetter and Wittinghofer, 2001*). To gain full insights into the dynamic switch between Sec14I3 forms, we examined the binding affinity of its interacting proteins with GTP γ S/GDP-loaded Sec14I3 *in vitro*. Results indicated that hFz5 had no preference for GDP- or GTP γ S-bound Sec14I3, while Dvl2 preferred binding to GDP-bound Sec14I3 (**Figure 6D,E and G**). On the contrary, Plc δ 4a showed much stronger interaction with GTP γ S-bound form (**Figure 6F–G**). These observations suggest that Dvl2 might participate in the switch of Sec14I3-GDP to Sec14I3-GTP, which then binds to and activates PLC.

Another important question is how active Sec14I3-GTP is cycled back to inactive Sec14I3-GDP. We speculated that Plc δ 4a, a binding partner of Sec14I3-GTP, might act as the GTPase-activating protein (GAP). To test this hypothesis, we compared the GTP hydrolysis activity of Sec14I3 in the presence and absence of Plc δ 4a protein. Results showed that the K_{hydr} rate was increased about 2.5-fold to $0.315 \pm 0.056 \text{ min}^{-1}$ in the presence of 94 nM Plc δ 4a, showing the GAP activity of Plc δ 4a (**Figure 6H**). Additionally, quantification of the K_{hydr} constants over different concentrations of Plc δ 4a determined its EC₅₀ value (50% of maximal effect value) as 21.3 nM (**Figure 6I**). On the other hand, our data disclosed that Plc δ 4a is incapable of stimulating GTP uptake by Sec14I3 (**Figure 6J**). Therefore, Plc δ 4a acts not only as a Sec14I3-GTP effector but as a terminator, a GAP of Sec14I3-GTP.

To verify the importance of the G α domain for the GTPase activity, full-length Sec14I3 and Sec14I3- Δ G α were purified from *E. coli*, and resuspended for steady-state GTPase activity assay. Results showed that full-length Sec14I3 stimulated the hydrolysis of GTP in a dose-dependent manner (data not shown), while Sec14I3- Δ G α exhibited the relatively low GTPase activity (**Figure 6K**), indicating the G α subunit actually engenders the GTPase activity of Sec14I3. Moreover, incubation with lysates from cells transfected with Δ G α form led to much higher levels of Plc δ 4a-PIP₂ association compared to the full-length form of Sec14I3 (**Figure 6L**); G α domain deletion had no effect on interaction with hFz5-CT, but impaired its binding to mDvl2 and Plc δ 4a (**Figure 6M** and **Figure 6—figure supplement 1A and B**). We speculate that the GTPase activity deficient Sec14I3- Δ G α is unable to bridge Dvl2 and Plc δ 4a for complex formation so that Plc δ 4a-bound PIP₂ may not be hydrolyzed due to PLC autoinhibition (*Hicks et al., 2008*).

Upregulation of PLC activity rescued sec14I3 deficiency-induced CE defects in embryos

To confirm that attenuated PLC/Ca²⁺ signaling was responsible for the phenotypes in Msec14I3 mutant embryos, we used U73122, an inhibitor of PLC (*Ashworth et al., 2007*), to test whether PLC inhibition phenocopies Msec14I3 mutants. Compared to the DMSO control, U73122 (1.5 μ M or 3

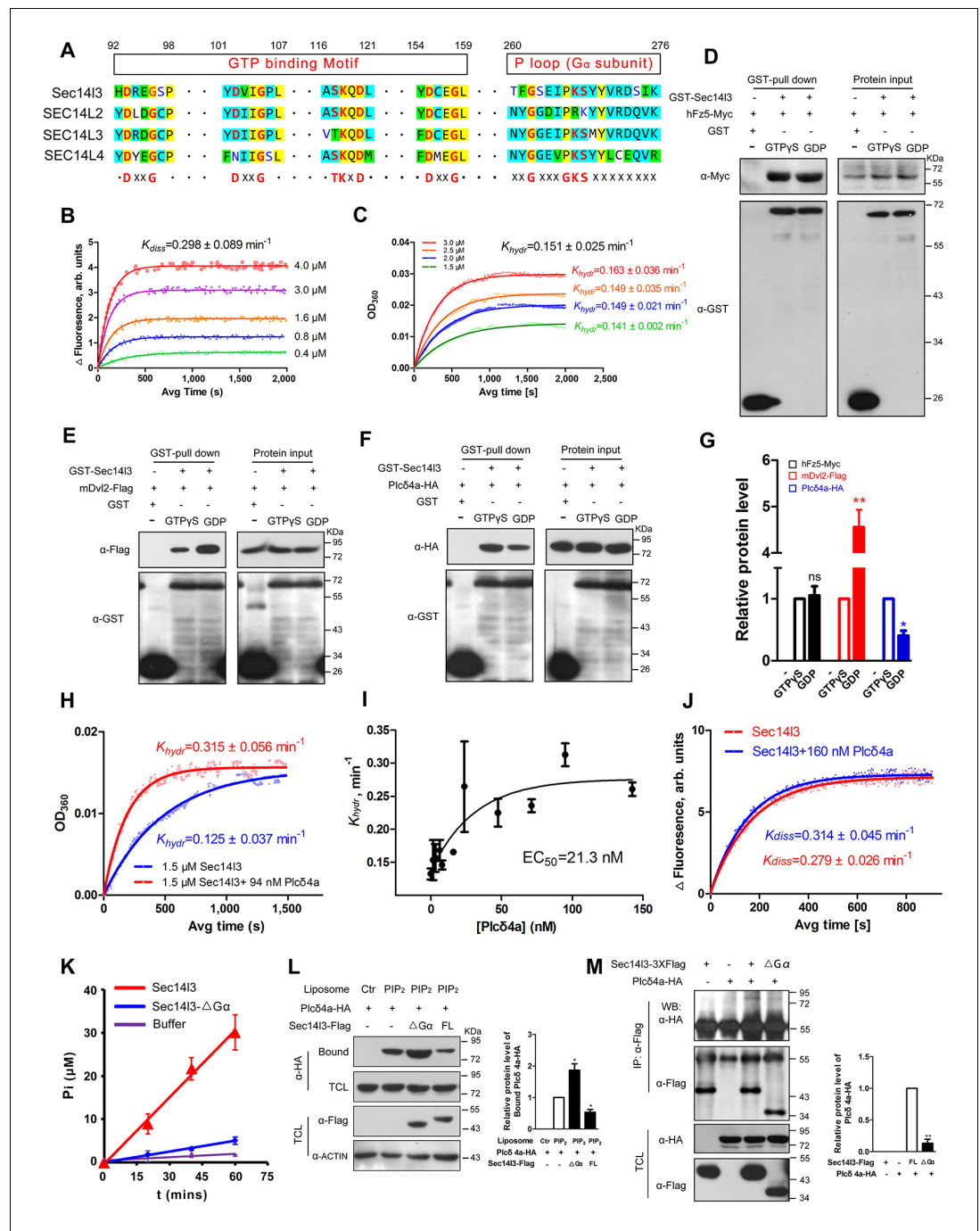


Figure 6. Sec143 exerts its GTPase activity to prime PLC. (A) Protein sequence alignment of zebrafish Sec143, and human SEC14L2, SEC14L3, and SEC14L4 in GTP binding motif and P loop region ($G\alpha$ subunit). Critical amino acids are highlighted in red as consensus at the last panel. (B) GTP binding activity of Sec143. The fluorescence of BODIPY-FL-GTP γ S at indicated concentrations was measured at room temperature ($\lambda_{ex} = 490$ nm and $\lambda_{em} = 510$ nm), following the addition of $10 \mu\text{M}$ Sec143. Data are representative uptake curves. The K_{diss} constant of Sec143 from three independent experiments is $0.298 \pm 0.089 \text{ min}^{-1}$. (C) GTP hydrolysis activity of Sec143. Time-course of Pi release from Sec143-GTP at indicated concentrations measured by absorbance at 360 nm in the single-turnover assay based on MESH system. Data are representative GTP hydrolysis curves and the K_{hydr} constant of Sec143 from three independent experiments is $0.151 \pm 0.025 \text{ min}^{-1}$. (D) Full-length hFz5 equally binds to GDP- and GTP γ S-bound Sec143 *in vitro*. (E) Full-length mDvl2 binds preferentially to inactive GDP-bound Sec143 *in vitro*. (F) Purified Plc δ 4a binds preferentially to active GTP γ S-bound Sec143 *in vitro*. (G) Quantification of relative protein level of hFz5-Myc (D), mDvl2-Flag (E) or Plc δ 4a-HA (F) bound by GST-Sec143 in the GTP γ S/GDP form. Data are Figure 6 continued on next page

Figure 6 continued

shown as mean \pm SEM from three separate experiments (** $p < 0.01$; $p < 0.05$; ns, non-significant). (H) Plc δ 4a functions as the GAP of Sec14I3. Data are representative GTP hydrolysis curves from three independent experiments. The K_{hydr} constant is statistically significant between two treatments with $p < 0.05$. (I) Quantification of the K_{hydr} constants over different concentrations of Plc δ 4a. Each concentration is plotted as mean \pm SEM from three independent experiments. (J) GTP binding activity of 10 μ M Sec14I3 in the absence or presence of 160 nM Plc δ 4a. Data shows an example of BODIPY-GTP γ S uptake curve of three experiments. These two K_{diss} constants have no significant difference by the Student's t test. (K) G α subunit deletion led to a decreased GTPase activity of Sec14I3. Data shown are representative curves out of three replicates and are plotted as mean \pm SEM. (L) Sec14I3- Δ G α protein overexpression disturbs Plc δ 4a-mediated PIP $_2$ degradation *in vitro*. Equal amounts of purified Plc δ 4a protein and liposomes containing PIP $_2$ or not were incubated with Sec14I3-transfected cell lysates. Liposome-bound Plc δ 4a was eluted and analyzed with quantification data as mean \pm SEM on the right (* $p < 0.05$). (M) G α subunit mediates Plc δ 4a interaction with Sec14I3 in HEK293T cells. Quantification data from three independent experiments are shown as mean \pm SEM on the right (** $p < 0.01$). All numerical data represented as a graph in the figure are shown in **Figure 6—source data 1**.

DOI: [10.7554/eLife.26362.021](https://doi.org/10.7554/eLife.26362.021)

The following source data and figure supplement are available for figure 6:

Source data 1. Numerical data for graphs in **Figure 6** and **Figure 6—figure supplement 1**.

DOI: [10.7554/eLife.26362.022](https://doi.org/10.7554/eLife.26362.022)

Figure supplement 1. G α subunit deletion had no effect on interaction with hFz5-CT, but impaired its binding to mDvl2.

DOI: [10.7554/eLife.26362.023](https://doi.org/10.7554/eLife.26362.023)

μ M) treatment at the 1 cell stage indeed postponed embryonic epiboly process, phenocopying Msec14I3 mutants (**Figure 7A**). Additionally, U73122 treatment caused a significant enhancement of PIP $_2$ accumulation at the PM at 4 and 6 hpf (**Figure 7B**), which phenocopied Msec14I3 mutants.

We explored a possibility to rescue Msec14I3 mutant phenotype by artificially activating PLC in mutants. We constructed an X/Y linker-truncated form of Plc δ 4a, Plc δ 4a- Δ 28, which was assumed to enhance the basal activity by relieving its autoinhibition (**Hicks et al., 2008**). Injection of plc δ 4a- Δ 28 mRNA into Msec14I3 mutant embryos partially rescued defects in morphology and CE marker gene expression (**Figure 7C**). So it is very likely that Plc δ 4a plays a role in gastrulation cell movements by mediating Sec14I3 effect in the Wnt/Ca $^{2+}$ signaling pathway.

Discussion

To date, only a few biochemical studies based on overexpression or inhibitors of proteins have suggested the implication of heterotrimeric G proteins in Wnt/Ca $^{2+}$ signaling (**Malbon, 2004; Katanaev et al., 2005; Schulte and Bryja, 2007**). However, it is unresolved as to how Fz/Dvl couples with G/GTPase proteins in Wnt/Ca $^{2+}$ signaling (**Sheldahl et al., 1999; Aznar et al., 2015; Schulte and Bryja, 2007**). In this study, we show that Sec14-like phosphatidylinositol transfer proteins can function as GTPase proteins in Wnt/Ca $^{2+}$ signaling. As modeled for Sec14I3 (**Figure 7D**), Sec14I3-GDP can form complexes with Fz and Dvl; in respond to non-canonical Wnt stimulation, activated Sec14I3-GTP associates with and activates PLC at the PM, and promotes PLC-mediated PIP $_2$ hydrolysis to generate second messengers that propagate the Wnt/Ca $^{2+}$ signaling cascade. In zebrafish, depletion of maternal sec14I3 impairs Wnt/Ca $^{2+}$ signaling transduction and consequently causes defective gastrulation cell movements. Our findings not only reveal a critical function for Sec14I3 in regulating Wnt/Ca $^{2+}$ signaling, but provide a comprehensive view of mechanisms about GTPase proteins involvement during the signaling transduction, breaking the argument whether the 7-TM Fz can directly bind to and activate G proteins. We propose it is the GTPase proteins, Sec14I3/SEC14L2, other than the classical heterotrimeric G proteins, that can simultaneously bind to upstream Fz/Dvl and activate downstream PLC for signal propagation. Therefore, the function of Sec14-like proteins is not limited to regulate the exchange of membrane lipids.

The direct Fz-Sec14I3 interaction can also be interpreted as Sec14I3-mediated regulation at the receptor level, such as Fz internalization or recycling in Wnt/Ca $^{2+}$ signaling (data not shown), which needs to be further investigated. Although our clues so far can't discriminate the transducer as a trimer or multimer, the organizer function of Sec14I3 in Wnt/Ca $^{2+}$ is recognizable. What's more, it has

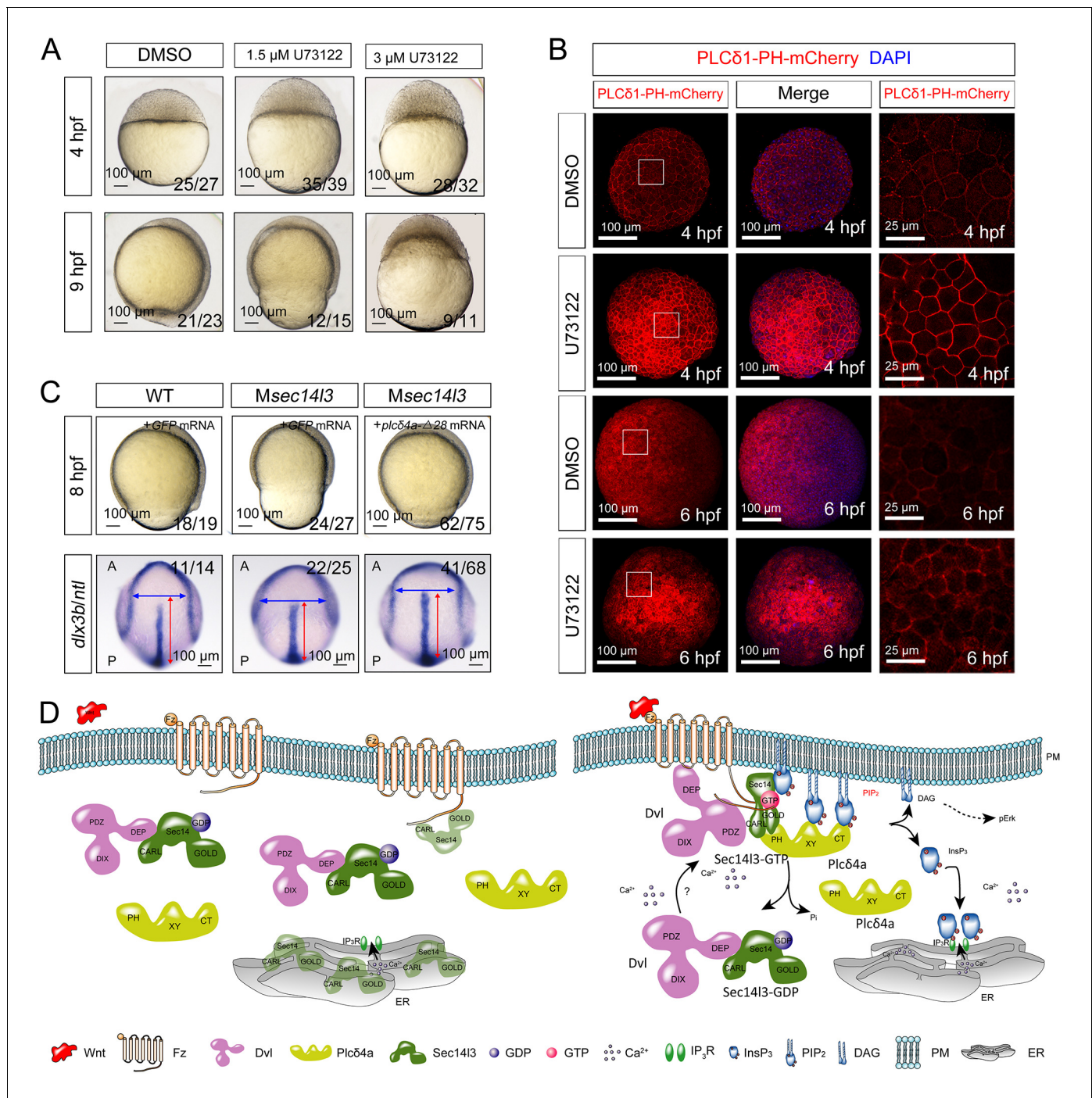


Figure 7. Sustained PLC activity partially rescues Msec14/3 defects. (A) Morphological defects in zebrafish embryos treated with 1.5 μ M or 3 μ M U73122 from the 1 cell stage. DMSO treated group serves as a control. Scale bars, 100 μ m. (B) Confocal imaging of PLC δ 1-PH-mCherry (red, PIP₂ probe) shows the PM accumulation of PIP₂ in zebrafish embryos treated with 1.5 μ M DMSO or 1.5 μ M U73122 at 4 and 6 hpf. The first two whole embryo panels are 3D views of z-stacks, while the last panel is enlarged views of single z-stack pictures (z = 5 for both 4 hpf and 6 hpf) from regions encompassed by white boxes. Scale bars, 100 μ m for the whole embryos; 25 μ m for the enlarged columns. (C) Active Plc δ 4a overcomes the CE defects in Msec14/3 mutants. 100 pg *plc δ 4a- Δ 28* mRNA was used for injection. Lateral views for embryos in the first panel, dorsal views for those in the last panel. Blue and red two-way arrows indicate the width of neural plate and the length of notochord respectively. Scale bars, 100 μ m. (D) Hypothetic working model of Sec14/3 participation in Wnt/Ca²⁺ signaling. In the absence of Wnt (left panel), Sec14/3 is mainly maintained in the ER and cytoplasm, forming a heterodimer with Dvl in its inactive state, Sec14/3-GDP. Upon Wnt5 stimulation (right panel), Fz/Dvl-mediated Sec14/3 is recruited to the PM and switched to the active state, Sec14/3-GTP, and subsequently promotes Plc δ 4a localization from cytoplasm to the PM and then the consequent activity at least in two

Figure 7 continued on next page

Figure 7 continued

aspects: its PIP₂ hydrolytic activity to generate second messenger InsP₃ and DAG for signaling propagation (Ca²⁺ release and p-Erk activation); and its GAP activity to terminate Sec14I3-GTP.

DOI: 10.7554/eLife.26362.024

been suggested that lipid transfer proteins may not simply function as diffusible vehicles mediating lipid transfer between membranes, but also devices of assigning PI lipids to various enzymatic reactions in a strictly regulated biological context (Mousley *et al.*, 2012). Our findings disclose multifaceted functions of lipid transfer proteins such as Sec14I3 and fill an important gap in our understanding of how Wnt/Fz/Dvl transduce the signal to PLC for Ca²⁺ release.

Although Sec14I3 is initially identified as a member of PITP, its depletion does not cause PIP₂ or PIP₃ reduction at the PM both in zebrafish embryos and mammalian cells. Our studies demonstrate that the depletion of Sec14I3 leads to PIP₂ accumulation at the PM due to inefficient activation of PLC. However, we cannot exclude the possibility of the involvement of Sec14I3 PI transfer activity in embryonic development because other PITP family members, such as Sestd1 and Sec14I1, are also highly expressed in zebrafish embryos (data not shown). Therefore, to investigate the intrinsic transfer activity of Sec14I3 during early embryogenesis, genetic analysis of double or triple mutants is necessary.

One of the most important aspects of our work is the discovery that the GTPase activity of Sec14I3 is critical for Plcδ4a activation. We find that Plcδ4a binds to Sec14I3-GTP with apparently higher affinity and functions as a Sec14I3-GAP protein. However, Sec14I3-GEF proteins remain unknown. Wnt receptor Fz is a kind of G protein-coupled receptors, which can act as GEF proteins for their cognate G proteins upon binding of a ligand (Malbon, 2004; Schulte and Bryja, 2007; Dijksterhuis *et al.*, 2014). We doubt that hFz5 or Rfz2 functions as the Sec14I3-GEF protein, because these Fz proteins show similar binding affinity towards GDP- or GTP-bound Sec14I3 and cannot accelerate the GTP uptake by Sec14I3 (Figure 6D,G and Figure 6—figure supplement 1C). Considering that Fz receptors can activate Gαi proteins and enhance Wnt/PCP signaling via the Dvl-binding protein, Daple, a novel non-receptor GEF (Aznar *et al.*, 2015; Ishida-Takagishi *et al.*, 2012), and Dvl2 does prefer to bind toward Sec14I3-GDP rather than Sec14I3-GTP in our hand (Figure 6E and G), we tend to believe that Dvl2 serves as a scaffolding protein to recruit an unknown Sec14I3-GEF, thereby enhancing Sec14I3-GTP formation. As for which is the particular GEF for Sec14I3 in Wnt/Ca²⁺ signaling transduction, more studies are needed. Besides, with the aid of available configuration-specific Sec14I3-GTP antibody in the future, it will be of great interest to figure out the conformational switches *in vivo*.

In summary, this study sheds light on a unique feature of the Sec14I3 protein. Through its intrinsic GTPase activity, it is capable of tightly coupling phospholipase activation with the proximity of PLC to its substrate. Moreover, these findings also provide the mechanism by which Dvl promotes calcium signaling.

Materials and methods

Embryos, injection and TALEN mutants generation

sec14I3 TALEN mutants were generated in the *Tg(flk:EGFP;gata1:dsRed)* (PRID:ZFIN_ZDB-FISH_150901_14755; ZFIN_ZDB_ALT_051223_6) transgenic fish using the FastTALE TALEN Assembly Kit (SiDanSai, Shanghai, China). The target site was near the start codon and included 22 bp both upstream and downstream (Figure 1—figure supplement 1C). To identify the candidate fishes with mutated alleles, genomic DNA was extracted from the tail and amplified using primer pairs as follows: the forward primer 5'-ccagcggcggagataaatc-3' and the reverse primer 5'-acatctatgacagacagcaatg-3'. The amplicons were purified for sequencing to determine the mutation types or digested with NlaIII to distinguish wild type and mutant embryos. The progenies derived from crosses between *sec14I3* heterozygotes were raised to adulthood, and homozygous mutant males and females were identified by genotyping. MZ*sec14I3* or M*sec14I3* mutant embryos were obtained by crossing homozygous mutant females to homozygous mutant males or wild-type males, respectively; Z*sec14I3* mutant embryos were obtained by crossing heterozygous females to heterozygous

males. Fishes were handled according to the institutional animal care and use committee (IACUC) protocol (AP#13-MAM1), which was approved and permitted by the Tsinghua University Animal Care and Use Committee. Embryos were staged according to *Kimmel et al. (1995)*.

Constructs

Zebrafish *sec14l3* and human *SEC14L2* full coding sequences were amplified using the following primers: *sec14l3* with 5'-CCGGAATTCATGAGCGGAAGGGTTGGAGATC-3' (forward) and 5'-CCGC TCGAGCTAGTTGTCTGATTGGTTGAC-3' (reverse), and *SEC14L2* with 5'-CCGGAATTCATGAGCGGCAGAGTCGGCGATC-3' (forward) and 5'-CCGCTCGAGTTATTCGGGGTGCCTGCC-3' (reverse). For information on the other constructs used in this study, please refer to the [Supplementary file 1](#).

mRNAs, morpholinos, and microinjection mRNAs were synthesized from corresponding linearized plasmids *in vitro* using a mMessage mMachine kit (Ambion/Thermo Fisher Scientific, Waltham, MA) and purified with RNeasy Mini Kit (QIAGEN, Duesseldorf, German). Morpholinos were synthesized by Gene Tools, LLC. The sequences of MOs used in our study are as follows: *sec14l3*-MO1, 5'-TCAGATCTCCAACCCCTCCGCTCAT-3'; *sec14l3*-MO2, 5'-ATGTCGCCACGAGTGCAGCAGAAAT-3'; *wnt5b*-MO1, 5'-GTCCTTGGTTCATTCTCACATCCAT-3'; and *std*-MO, 5'-CCTCTTACCTCAGTCAATTTATA-3'. About 1–1.5 nl of mRNA (or morpholino solution) was injected into the yolk at the 1 cell stage for ubiquitous expression or into one single cell at the 16–32 cell stage for clonal expression using the typical MPPI-2 quantitative injection equipment (Applied Scientific Instrumentation Co., Eugene, OR). The injection dose was the amount of the mRNA or morpholino received by a single embryo.

Whole-mount in situ hybridization and immunofluorescence

Whole-mount in situ hybridization was performed essentially following a standard protocol. Digoxigenin-UTP-labeled antisense RNA probes for detecting *dlx3b* and *ntl* mRNA were generated *in vitro* using a linearized plasmid (*Huang et al., 2007*). Following in situ hybridization, the embryos were immersed in glycerol and photographed using the Ds-Ri1 CCD camera under a Nikon SMZ1500 stereoscope. Embryonic immunofluorescence was carried out as previously described (*Zhang et al., 2012*), and the following antibodies were used: rabbit anti-p-Erk (Thr202/Tyr204) (Cell Signaling Technology, Danvers, MA, #9101, RRID:AB_331646), rabbit anti-p-Akt (Ser473) (Cell Signaling Technology, #4060, RRID:AB_2315049), mouse anti-SEC14L2 (ORIGENE, Rockville, MD, TA503723, RRID:AB_11126641), phalloidin (Sigma, St. Louis, MO, p1951, RRID:AB_2315148). Immunostained embryos were imaged under Nikon A1RMPSi lasers scanning confocal microscope using z-stack devices with 3.5 μm interval. And whole embryo images are 3D views of z-stacks, while the magnified images are pictures of a single z plane snap.

Cell culture, transfection and stable cell line establishment

HEK293T cells (RRID:CVCL_0063) were cultured in DMEM (Life Technologies) supplemented with 10% FBS (Hyclone, Logan, UT) and 50 $\mu\text{g}/\text{ml}$ penicillin/streptomycin (PS) (Invitrogen). PC3 cells (RRID:CVCL_0035) were cultured in F12K with 10% FBS and 50 $\mu\text{g}/\text{ml}$ PS. All cell lines were obtained from the Cell Resource Center, Peking Union Medical College (which is the headquarters of National Infrastructure of Cell Line Resource, NSTI). Cell lines were checked for free of mycoplasma contamination by PCR and culture. Its species origin was confirmed with PCR. The identity of the cell line was authenticated with STR profiling (FBI, CODIS). All the results can be viewed on the website (<http://cellresource.cn>). Transfections were performed using the polyethylenimine method. To establish human *SEC14L2* knockdown stable cell line, negative control shRNA (SHC016) and *SEC14L2* shRNA (TRCN0000019589, TRCN0000019590) plasmids (ordered from Sigma) were transfected into HEK293T/PC3 cells and then transfected cells were selected with puromycin (1 $\mu\text{g}/\text{ml}$). Following removal of the puromycin, the cells were allowed to recover and expand in regular growth medium and then were screened by protein immunoblotting. For serum starvation, cells were incubated in culture media in the absence of any additional supplements for 16 hr.

Imaging of calcium levels in embryos and cytosolic calcium measurements by flow cytometry

To image calcium levels in embryos, pXT7-GCaMP6 plasmid was constructed based on pGP-CMV-GCaMP6 and linearized for GCaMP6 mRNA labelling. Then GCaMP6 mRNA was mixed with Rhodamine and injected into 1 cell stage embryos, which were embed in low-melting agar at the indicated stages for time lapse imaging. Then the resulting images were treated to generate pseudocolor ratio images as previously described (*Slusarski et al., 1997b, 1997a*).

For calcium measurements in PC3 cells, cells were transfected with indicated plasmids for three days and loaded with calcium dye Quest Fluo 8-AM (AAT Bioquest, Sunnyvale, CA, 21083) or Rhod2-AM (AAT 21064) before flow cytometry analysis. During analysis, baseline fluorescence was measured for 50 s and stopped for Wnt5a addition, then measurement was resumed immediately for a total of 200s.

Western Blot, co-immunoprecipitations, immunostaining and GST pull-downs

Western blots, co-IPs and immunostaining were performed as previously described (*Zhang et al., 2009*). For two-step of Co-IPs, the first step Co-IP components were eluted with the reduced glutathione for the second step immunoprecipitation experiments. Staining of PIP₂ in the PM was carried out according to a protocol previously published by *Hammond et al. (2009)*. Fluorescent images were acquired using a Nikon A1RMPsi lasers scanning confocal microscope. The following commercial antibodies were used in this study: anti-Flag (F1804, Sigma, RRID:AB_262044), anti-HA (sc-7392, Santa Cruz, Dalls, TX, RRID:AB_627809), anti-Myc (sc-40AC, Santa Cruz, RRID:AB_627268), anti-GFP (sc-9996, Santa Cruz, RRID:AB_627695) and anti-hDVL2 (#3216, CST, RRID:AB_2093338). Wnt3a (5036-WN), Wnt5a (645-WN) and Wnt11 (6179-WN) ligands were purchased from R&D (Minneapolis, MN). For GST pull-down assay, GST-Plcδ4a-HA and GST-Sec14I3 fusion proteins were expressed in *E.coli* and purified using glutathione-Sepharose beads (GE Healthcare, Marlborough, MA). After washing with PBS, GST-Plcδ4a-HA beads were incubated with PreScission Protease (GE Healthcare) to remove the GST tag and the resulting Plcδ4a-HA was harvested by PBS elution. The GST-Sec14I3 beads were washed with PBS and then incubated with the purified Plcδ4a-HA fusion protein for 2 hr at 4°C, and then washed with PBS again. The final eluent was analyzed by western blot using anti-GST and anti-HA antibodies. For GTPγS/GDP-Sec14I3 pull down assay, immobilized GST-Sec14I3 protein (on glutathione-Sepharose beads) was prepared and incubated with binding buffer (50 mM Tris-HCl [pH 7.4], 100 mM NaCl, 0.4% [vol:vol] Nonidet P-40, 10 mM MgCl₂, 5 mM EDTA, 30 μM GTPγS /GDP, 2 mM DTT, protease inhibitor mixture) for 90 mins at room temperature as described before (*Wu et al., 1993; Aznar et al., 2015*). Then lysates of HEK293T cells with hFz5-Myc or mDvl2-Flag plasmid transfection or purified Plcδ4a-HA (5 μg) protein were added and rotated at 4°C for another 2 hr. Beads were then washed using wash buffer (4.3 mM Na₂HPO₄, 1.4 mM KH₂PO₄ [pH 7.4], 137 mM NaCl, 2.7 mM KCl, 0.1% [vol:vol] Tween 20, 10 mM MgCl₂, 5 mM EDTA, 30 μM GTPγS /GDP, 2 mM DTT) for 4 times every 3 min, finally boiled in 2xloading buffer for SDS-PAGE using corresponding antibodies.

Liposome binding and membrane isolation assays

For the liposome binding assay, 1 μg HA-tagged Plcδ4a protein purified from *E. coli*, 20 μl 1 mM PolyPIPosomes (Echelon Biosciences, Salt Lake City, UT, Y-0000 and Y-P045), none or 5% PIP₂, 500 μl cell lysates transfected with control shRNA or *SEC14L2* shRNA and 500 μl binding buffer (50 mM Tris, pH 7.5, 150 mM NaCl, 0.05% NonidetP-40) were mixed and rotated for 4 hr at 4°C and then centrifuged at 13,000 rpm for 10 min. The liposome pellet was then washed with 1 ml of binding buffer (50 mM Tris, pH 7.5, 150 mM NaCl, 0.05% NonidetP-40) for three times. The bound and flow-through samples were eluted in 2xSDS loading buffer, separated by SDS-PAGE, transferred to nitrocellulose, and then Plcδ4a levels were measured by immunoblot with anti-HA antibody.

For the membrane isolation assay, a Minute™ Plasma Membrane Protein Isolation Kit (Invent Biotechnologies, Inc., Plymouth, MN, Catalog number: SM-005) was used according to the manufacturer's instructions. The isolated membrane samples were then dissolved in 2xSDS loading buffer and detected by separated by western blot using appropriate antibodies.

GTP binding and hydrolysis assays

GTP binding and hydrolysis activity are measured using BODIPY-FL-GTP γ S conventional assay and MESG-based single-turnover assay respectively; BODIPY-FL-GTP γ S conventional assay is based on the release of the fluorescence quenching of BODIPY-FL-GTP γ S (a non-hydrolyzable GTP analog) upon its binding to G proteins. BODIPY-FL-GTP γ S (Invitrogen, G22183) binding to recombinant Sec14I3 was determined in 10 mM HEPES (pH 8.0), 1 mM EDTA and 10 mM MgCl₂ (HEM buffer). The fluorescence ($\lambda_{\text{ex}} = 490$ nm and $\lambda_{\text{em}} = 510$ nm) was monitored for samples at different concentrations of BODIPY-FL-GTP γ S, following the addition of 10 μ M Sec14I3 protein, in a fluorescence microplate reader (Thermo Scientific VARIOSKAN FLASH). For the kinetic experiments, fluorescence of BODIPY-FL-GTP γ S alone was measured in HEM at room temperature for 3 min and then binding was initiated with addition of excess Sec14I3. The change in fluorescence was measured over time and fitted with one phase exponential equation: $a*(1-e^{-kt})$ to obtain the K_{diss} constant using GraphPad Prism 5.

The hydrolysis of GTP by Sec14I3 was measured by the MESG system monitoring the time course absorbance at 360 nm. The reaction was determined in 100 μ l solution containing 50 mM MOPs (pH 7.0), 1 mM EDTA, 200 mM GTP, 1 U/ml purine nucleoside phosphorylase, 0.2 mM MESG and the recombinant Sec14I3 protein (reconstituted in Tris-HCl buffer). Single-turnover GTPase reactions were initiated by adding of MgCl₂ to a final concentration of 5 mM using the injector unit followed by immediate measurement (Thermo Scientific VARIOSKAN FLASH). The hydrolysis data fitted with one phase exponential equation: $a*(1-e^{-kt})$ to obtain the K_{hydr} constant using GraphPad Prism 5. The time-course of Pi release from Sec14I3-GTP at four different concentrations was monitored, and finally averaged to determine the K_{hydr} constant of Sec14I3.

For measurements of Plc δ 4a GAP functions, indicated amounts of GAP proteins were mixed with Sec14I3 before MgCl₂ initiation, and control experiments with indicated GAP proteins were carried out to provide a background of absorbance in each independent measurement to be subtracted from the sample signals.

Steady-state GTPase activity was performed using a QuantiChrom ATPase/GTPase Assay kit (GENTAUR, San Jose, CA, DATG-200) according to the manufacturer's instructions.

Statistical analysis

Quantitative data are presented as mean \pm SEM, and comparisons were performed between groups using a two-tailed Student's t-test. For all analyses, * $p < 0.05$; ** $p < 0.01$ were considered statistically significant; ns indicated statistical non-significance with $p > 0.05$. Each experiment was carried out at least three times independently.

Acknowledgements

We thank Jiawei Wu and Jue Wang for help with MESG-based single-turnover assay, Wei Wu for providing hFz5-Myc, Bailong Xiao for STIM1-mCherry, Douglas Kim for pGP-CMV-GCaMP6 (Addgene plasmid #40753) and Randall Moon for XE128 Rfz2 TG2myc CS2+ (Addgene plasmid #16796). We are grateful to the members of the Meng Laboratory and Drs. Qiang Wang and Wei Wu for helpful discussion and technical assistance. This work was financially supported by grants from the National Natural Science Foundation of China (#31522035 and #31371460), Ministry of Science and Technology of the People's Republic of China (#2012CB945100, #2011CB943800).

Additional information

Funding

Funder	Grant reference number	Author
National Natural Science Foundation of China	31522035	Shunji Jia
National Natural Science Foundation of China	31371460	Shunji Jia
Ministry of Science and Tech-	2012CB945100	Shunji Jia

nology of the People's Republic of China

Ministry of Science and Technology of the People's Republic of China 2011CB943800

Anming Meng

The funders had no role in study design, data collection and interpretation, or the decision to submit the work for publication.

Author contributions

BG, Data curation, Software, Formal analysis, Validation, Investigation, Methodology, Writing—original draft; WS, Software, Visualization, Methodology; WX, Resources, Visualization, Methodology; YM, Visualization, Methodology; AM, Conceptualization, Supervision, Validation, Project administration, Writing—review and editing; SJ, Supervision, Funding acquisition, Validation, Methodology, Writing—original draft, Project administration, Writing—review and editing

Author ORCIDs

Shunji Jia,  <http://orcid.org/0000-0001-8678-1714>

Ethics

Animal experimentation: Fishes were handled according to the institutional animal care and use committee (IACUC) protocols (AP#13-MAM1), which were approved and permitted by the Tsinghua University Animal Care and Use Committee.

Additional files

Supplementary files

- Supplementary file 1. Primers used in the present study.

DOI: [10.7554/eLife.26362.025](https://doi.org/10.7554/eLife.26362.025)

References

- Allen-Baume V, Ségui B, Cockcroft S. 2002. Current thoughts on the phosphatidylinositol transfer protein family. *FEBS Letters* **531**:74–80. doi: [10.1016/S0014-5793\(02\)03412-9](https://doi.org/10.1016/S0014-5793(02)03412-9), PMID: [12401207](https://pubmed.ncbi.nlm.nih.gov/12401207/)
- Angers S, Moon RT. 2009. Proximal events in wnt signal transduction. *Nature Reviews Molecular Cell Biology* **10**:468–477. doi: [10.1038/nrm2717](https://doi.org/10.1038/nrm2717), PMID: [19536106](https://pubmed.ncbi.nlm.nih.gov/19536106/)
- Ashworth R, Devogelaere B, Fabes J, Tunwell RE, Koh KR, De Smedt H, Patel S. 2007. Molecular and functional characterization of inositol trisphosphate receptors during early zebrafish development. *Journal of Biological Chemistry* **282**:13984–13993. doi: [10.1074/jbc.M700940200](https://doi.org/10.1074/jbc.M700940200), PMID: [17331947](https://pubmed.ncbi.nlm.nih.gov/17331947/)
- Aznar N, Midde KK, Dunkel Y, Lopez-Sanchez I, Pavlova Y, Marivin A, Barbazán J, Murray F, Nitsche U, Janssen KP, Willert K, Goel A, Abal M, Garcia-Marcos M, Ghosh P. 2015. Daple is a novel non-receptor GEF required for trimeric G protein activation in Wnt signaling. *eLife* **4**:e07091. doi: [10.7554/eLife.07091](https://doi.org/10.7554/eLife.07091), PMID: [26126266](https://pubmed.ncbi.nlm.nih.gov/26126266/)
- Cha SW, Tadjuidje E, Tao Q, Wylie C, Heasman J. 2008. Wnt5a and Wnt11 interact in a maternal Dkk1-regulated fashion to activate both canonical and non-canonical signaling in xenopus Axis formation. *Development* **135**:3719–3729. doi: [10.1242/dev.029025](https://doi.org/10.1242/dev.029025), PMID: [18927149](https://pubmed.ncbi.nlm.nih.gov/18927149/)
- Chen TW, Wardill TJ, Sun Y, Pulver SR, Renninger SL, Baohan A, Schreiter ER, Kerr RA, Orger MB, Jayaraman V, Looger LL, Svoboda K, Kim DS. 2013. Ultrasensitive fluorescent proteins for imaging neuronal activity. *Nature* **499**:295–300. doi: [10.1038/nature12354](https://doi.org/10.1038/nature12354), PMID: [23868258](https://pubmed.ncbi.nlm.nih.gov/23868258/)
- Clevers H, Nusse R. 2012. Wnt/ β -catenin signaling and disease. *Cell* **149**:1192–1205. doi: [10.1016/j.cell.2012.05.012](https://doi.org/10.1016/j.cell.2012.05.012), PMID: [22682243](https://pubmed.ncbi.nlm.nih.gov/22682243/)
- Cockcroft S. 2012. The diverse functions of phosphatidylinositol transfer proteins. *Current Topics in Microbiology and Immunology* **362**:185–208. doi: [10.1007/978-94-007-5025-8_9](https://doi.org/10.1007/978-94-007-5025-8_9), PMID: [23086419](https://pubmed.ncbi.nlm.nih.gov/23086419/)
- Dijksterhuis JP, Petersen J, Schulte G. 2014. WNT/Frizzled signalling: receptor-ligand selectivity with focus on FZD-G protein signalling and its physiological relevance: iuphar Review 3. *British Journal of Pharmacology* **171**:1195–1209. doi: [10.1111/bph.12364](https://doi.org/10.1111/bph.12364), PMID: [24032637](https://pubmed.ncbi.nlm.nih.gov/24032637/)
- Flock T, Ravarani CN, Sun D, Venkatakrishnan AJ, Kayikci M, Tate CG, Veprintsev DB, Babu MM. 2015. Universal allosteric mechanism for α activation by GPCRs. *Nature* **524**:173–179. doi: [10.1038/nature14663](https://doi.org/10.1038/nature14663), PMID: [26147082](https://pubmed.ncbi.nlm.nih.gov/26147082/)
- Foldynová-Trantírková S, Sekyrová P, Tmejová K, Brumovská E, Bernatík O, Blankenfeldt W, Krejčí P, Kozubík A, Dolezal T, Trantírek L, Bryja V. 2010. Breast cancer-specific mutations in CK1epsilon inhibit Wnt/beta-catenin

- and activate the Wnt/Rac1/JNK and NFAT pathways to decrease cell adhesion and promote cell migration. *Breast Cancer Research* **12**:R30. doi: [10.1186/bcr2581](https://doi.org/10.1186/bcr2581), PMID: 20507565
- Habermehl D**, Kempna P, Azzi A, Zingg JM. 2005. Recombinant SEC14-like proteins (TAP) possess GTPase activity. *Biochemical and Biophysical Research Communications* **326**:254–259. doi: [10.1016/j.bbrc.2004.11.021](https://doi.org/10.1016/j.bbrc.2004.11.021), PMID: 15567179
- Halleskog C**, Dijksterhuis JP, Kilander MB, Becerril-Ortega J, Villaescusa JC, Lindgren E, Arenas E, Schulte G. 2012. Heterotrimeric G protein-dependent WNT-5A signaling to ERK1/2 mediates distinct aspects of microglia proinflammatory transformation. *Journal of Neuroinflammation* **9**:111. doi: [10.1186/1742-2094-9-111](https://doi.org/10.1186/1742-2094-9-111), PMID: 22647544
- Halleskog C**, Schulte G. 2013. Pertussis toxin-sensitive heterotrimeric G(α /o) proteins mediate WNT/ β -catenin and WNT/ERK1/2 signaling in mouse primary microglia stimulated with purified WNT-3A. *Cellular Signalling* **25**:822–828. doi: [10.1016/j.cellsig.2012.12.006](https://doi.org/10.1016/j.cellsig.2012.12.006), PMID: 23266471
- Hammond GR**, Schiavo G, Irvine RF. 2009. Immunocytochemical techniques reveal multiple, distinct cellular pools of PtdIns4P and PtdIns(4,5)P(2). *Biochemical Journal* **422**:23–35. doi: [10.1042/BJ20090428](https://doi.org/10.1042/BJ20090428), PMID: 19508231
- Hicks SN**, Jczyk MR, Gershburg S, Seifert JP, Harden TK, Sondek J. 2008. General and versatile autoinhibition of PLC isozymes. *Molecular Cell* **31**:383–394. doi: [10.1016/j.molcel.2008.06.018](https://doi.org/10.1016/j.molcel.2008.06.018), PMID: 18691970
- Huang H**, Lu FI, Jia S, Meng S, Cao Y, Wang Y, Ma W, Yin K, Wen Z, Peng J, Thisse C, Thisse B, Meng A. 2007. Amotl2 is essential for cell movements in zebrafish embryo and regulates c-Src translocation. *Development* **134**:979–988. doi: [10.1242/dev.02782](https://doi.org/10.1242/dev.02782), PMID: 17293535
- Huelsken J**, Birchmeier W. 2001. New aspects of Wnt signaling pathways in higher vertebrates. *Current Opinion in Genetics & Development* **11**:547–553. doi: [10.1016/S0959-437X\(00\)00231-8](https://doi.org/10.1016/S0959-437X(00)00231-8), PMID: 11532397
- Idevall-Hagren O**, De Camilli P. 2015. Detection and manipulation of phosphoinositides. *Biochimica Et Biophysica Acta (BBA) - Molecular and Cell Biology of Lipids* **1851**:736–745. doi: [10.1016/j.bbalip.2014.12.008](https://doi.org/10.1016/j.bbalip.2014.12.008), PMID: 25514766
- Ishida-Takagishi M**, Enomoto A, Asai N, Ushida K, Watanabe T, Hashimoto T, Kato T, Weng L, Matsumoto S, Asai M, Murakumo Y, Kaibuchi K, Kikuchi A, Takahashi M. 2012. The Dishevelled-associating protein duple controls the non-canonical Wnt/Rac pathway and cell motility. *Nature Communications* **3**:859. doi: [10.1038/ncomms1861](https://doi.org/10.1038/ncomms1861), PMID: 22643886
- Kadamur G**, Ross EM. 2013. Mammalian phospholipase C. *Annual Review of Physiology* **75**:127–154. doi: [10.1146/annurev-physiol-030212-183750](https://doi.org/10.1146/annurev-physiol-030212-183750), PMID: 23140367
- Katanaev VL**, Ponzielli R, Sémériva M, Tomlinson A. 2005. Trimeric G protein-dependent frizzled signaling in *Drosophila*. *Cell* **120**:111–122. doi: [10.1016/j.cell.2004.11.014](https://doi.org/10.1016/j.cell.2004.11.014), PMID: 15652486
- Kauffmann-Zeh A**, Thomas GM, Ball A, Prosser S, Cunningham E, Cockcroft S, Hsuan JJ. 1995. Requirement for phosphatidylinositol transfer protein in epidermal growth factor signaling. *Science* **268**:1188–1190. doi: [10.1126/science.7761838](https://doi.org/10.1126/science.7761838), PMID: 7761838
- Kearns BG**, Alb JG, Bankaitis V. 1998. Phosphatidylinositol transfer proteins: the long and winding road to physiological function. *Trends in Cell Biology* **8**:276–282. doi: [10.1016/S0962-8924\(98\)01281-1](https://doi.org/10.1016/S0962-8924(98)01281-1), PMID: 9714599
- Kimmel CB**, Ballard WW, Kimmel SR, Ullmann B, Schilling TF. 1995. Stages of embryonic development of the zebrafish. *Developmental Dynamics* **203**:253–310. doi: [10.1002/aja.1002030302](https://doi.org/10.1002/aja.1002030302), PMID: 8589427
- Kohn AD**, Moon RT. 2005. Wnt and calcium signaling: beta-catenin-independent pathways. *Cell Calcium* **38**:439–446. doi: [10.1016/j.ceca.2005.06.022](https://doi.org/10.1016/j.ceca.2005.06.022), PMID: 16099039
- Komiya Y**, Habas R. 2008. Wnt signal transduction pathways. *Organogenesis* **4**:68–75. doi: [10.4161/org.4.2.5851](https://doi.org/10.4161/org.4.2.5851)
- Kühl M**, Sheldahl LC, Park M, Miller JR, Moon RT. 2000a. The Wnt/Ca²⁺ pathway. *Trends in Genetics* **16**:279–283. doi: [10.1016/S0168-9525\(00\)02028-X](https://doi.org/10.1016/S0168-9525(00)02028-X)
- Kühl M**, Sheldahl LC, Park M, Miller JR, Moon RT. 2000b. The Wnt/Ca²⁺ pathway: a new vertebrate Wnt signaling pathway takes shape. *Trends in Genetics* **16**:279–283. doi: [10.1016/S0168-9525\(00\)02028-X](https://doi.org/10.1016/S0168-9525(00)02028-X), PMID: 10858654
- Kühl M**, Geis K, Sheldahl LC, Pukrop T, Moon RT, Wedlich D. 2001. Antagonistic regulation of convergent extension movements in *Xenopus* by Wnt/ β -catenin and Wnt/Ca²⁺ signaling. *Mechanisms of Development* **106**:61–76. doi: [10.1016/S0925-4773\(01\)00416-6](https://doi.org/10.1016/S0925-4773(01)00416-6), PMID: 11472835
- Lin S**, Baye LM, Westfall TA, Slusarski DC. 2010. Wnt5b-Ryk pathway provides directional signals to regulate gastrulation movement. *The Journal of Cell Biology* **190**:263–278. doi: [10.1083/jcb.200912128](https://doi.org/10.1083/jcb.200912128), PMID: 20660632
- Lin C**, Koval A, Tishchenko S, Gabdulkhakov A, Tin U, Solis GP, Katanaev VL. 2014. Double suppression of the α protein activity by RGS proteins. *Molecular Cell* **53**:663–671. doi: [10.1016/j.molcel.2014.01.014](https://doi.org/10.1016/j.molcel.2014.01.014), PMID: 24560274
- Liou J**, Kim ML, Heo WD, Jones JT, Myers JW, Ferrell JE, Meyer T. 2005. STIM is a Ca²⁺ sensor essential for Ca²⁺-store-depletion-triggered Ca²⁺ influx. *Current Biology* **15**:1235–1241. doi: [10.1016/j.cub.2005.05.055](https://doi.org/10.1016/j.cub.2005.05.055), PMID: 16005298
- Liu T**, Liu X, Wang H, Moon RT, Malbon CC. 1999. Activation of rat frizzled-1 promotes Wnt signaling and differentiation of mouse F9 teratocarcinoma cells via pathways that require galph α (q) and galph α (o) function. *Journal of Biological Chemistry* **274**:33539–33544. doi: [10.1074/jbc.274.47.33539](https://doi.org/10.1074/jbc.274.47.33539), PMID: 10559239
- Loh KM**, van Amerongen R, Nusse R. 2016. Generating Cellular Diversity and spatial form: Wnt signaling and the evolution of multicellular animals. *Developmental Cell* **38**:643–655. doi: [10.1016/j.devcel.2016.08.011](https://doi.org/10.1016/j.devcel.2016.08.011), PMID: 27676437
- MacDonald BT**, Tamai K, He X. 2009. Wnt/ β -catenin signaling: components, mechanisms, and diseases. *Developmental Cell* **17**:9–26. doi: [10.1016/j.devcel.2009.06.016](https://doi.org/10.1016/j.devcel.2009.06.016), PMID: 19619488

- Malbon CC.** 2004. Frizzleds: new members of the superfamily of G-protein-coupled receptors. *Frontiers in Bioscience* **9**:1048–1058. doi: [10.2741/1308](https://doi.org/10.2741/1308), PMID: [14977528](https://pubmed.ncbi.nlm.nih.gov/14977528/)
- McEwen DP, Gee KR, Kang HC, Neubig RR.** 2001. Fluorescent BODIPY-GTP analogs: real-time measurement of nucleotide binding to G proteins. *Analytical Biochemistry* **291**:109–117. doi: [10.1006/abio.2001.5011](https://doi.org/10.1006/abio.2001.5011), PMID: [11262163](https://pubmed.ncbi.nlm.nih.gov/11262163/)
- Merkulova MI, Andreeva SG, Shuvaeva TM, Novoselov SV, Peshenko IV, Bystrova MF, Novoselov VI, Fesenko EE, Lipkin VM.** 1999. A novel 45 kDa secretory protein from rat olfactory epithelium: primary structure and localisation. *FEBS Letters* **450**:126–130. doi: [10.1016/S0014-5793\(99\)00470-6](https://doi.org/10.1016/S0014-5793(99)00470-6), PMID: [10350070](https://pubmed.ncbi.nlm.nih.gov/10350070/)
- Mikels AJ, Nusse R.** 2006. Purified Wnt5a protein activates or inhibits beta-catenin-TCF signaling depending on receptor context. *PLoS Biology* **4**:e115. doi: [10.1371/journal.pbio.0040115](https://doi.org/10.1371/journal.pbio.0040115), PMID: [16602827](https://pubmed.ncbi.nlm.nih.gov/16602827/)
- Mousley CJ, Davison JM, Bankaitis VA.** 2012. Sec14 like PITPs couple lipid metabolism with phosphoinositide synthesis to regulate golgi functionality. *Sub-Cellular Biochemistry* **59**:271–287. doi: [10.1007/978-94-007-3015-1_9](https://doi.org/10.1007/978-94-007-3015-1_9), PMID: [22374094](https://pubmed.ncbi.nlm.nih.gov/22374094/)
- Nakai J, Ohkura M, Imoto K.** 2001. A high signal-to-noise ca(2+) probe composed of a single green fluorescent protein. *Nature Biotechnology* **19**:137–141. doi: [10.1038/84397](https://doi.org/10.1038/84397), PMID: [11175727](https://pubmed.ncbi.nlm.nih.gov/11175727/)
- Niehrs C.** 2012. The complex world of WNT receptor signalling. *Nature Reviews Molecular Cell Biology* **13**:767–779. doi: [10.1038/nrm3470](https://doi.org/10.1038/nrm3470), PMID: [23151663](https://pubmed.ncbi.nlm.nih.gov/23151663/)
- Nile AH, Bankaitis VA, Grabon A.** 2010. Mammalian diseases of phosphatidylinositol transfer proteins and their homologs. *Clinical Lipidology* **5**:867–897. doi: [10.2217/clp.10.67](https://doi.org/10.2217/clp.10.67), PMID: [21603057](https://pubmed.ncbi.nlm.nih.gov/21603057/)
- Novoselov VI, Peshenko IV, Evdokimov VJ, Nikolaev JV, Matveeva EA, Fesenko EE.** 1994. Water-soluble GTP-binding protein from rat olfactory epithelium. *FEBS Letters* **353**:286–288. doi: [10.1016/0014-5793\(94\)01051-X](https://doi.org/10.1016/0014-5793(94)01051-X), PMID: [7957876](https://pubmed.ncbi.nlm.nih.gov/7957876/)
- Novoselov VI, Peshenko IV, Evdokimov VA, Nikolaev JV, Matveeva EA, Fesenko EE.** 1996. 45-kDa GTP-binding protein from rat olfactory epithelium: purification, characterization and localization. *Chemical Senses* **21**:181–188. doi: [10.1093/chemse/21.2.181](https://doi.org/10.1093/chemse/21.2.181), PMID: [8670696](https://pubmed.ncbi.nlm.nih.gov/8670696/)
- Oner SS, Maher EM, Gabay M, Tall GG, Blumer JB, Lanier SM.** 2013. Regulation of the G-protein regulatory-Gαi signaling complex by nonreceptor guanine nucleotide exchange factors. *Journal of Biological Chemistry* **288**:3003–3015. doi: [10.1074/jbc.M112.418467](https://doi.org/10.1074/jbc.M112.418467), PMID: [23212907](https://pubmed.ncbi.nlm.nih.gov/23212907/)
- Rhee SG.** 2001. Regulation of phosphoinositide-specific phospholipase C. *Annual Review of Biochemistry* **70**:281–312. doi: [10.1146/annurev.biochem.70.1.281](https://doi.org/10.1146/annurev.biochem.70.1.281), PMID: [11395409](https://pubmed.ncbi.nlm.nih.gov/11395409/)
- Schulte G, Bryja V.** 2007. The frizzled family of unconventional G-protein-coupled receptors. *Trends in Pharmacological Sciences* **28**:518–525. doi: [10.1016/j.tips.2007.09.001](https://doi.org/10.1016/j.tips.2007.09.001), PMID: [17884187](https://pubmed.ncbi.nlm.nih.gov/17884187/)
- Seitz K, Dürsch V, Harnoš J, Bryja V, Gentzel M, Schambony A.** 2014. β-Arrestin interacts with the beta/gamma subunits of trimeric G-proteins and dishevelled in the wnt/Ca(2+) pathway in xenopus gastrulation. *PLoS One* **9**:e87132. doi: [10.1371/journal.pone.0087132](https://doi.org/10.1371/journal.pone.0087132), PMID: [24489854](https://pubmed.ncbi.nlm.nih.gov/24489854/)
- Semenov MV, Habas R, Macdonald BT, He X.** 2007. SnapShot: noncanonical Wnt signaling Pathways. *Cell* **131**:1378–1378. doi: [10.1016/j.cell.2007.12.011](https://doi.org/10.1016/j.cell.2007.12.011), PMID: [18160045](https://pubmed.ncbi.nlm.nih.gov/18160045/)
- Sheldahl LC, Park M, Malbon CC, Moon RT.** 1999. Protein kinase C is differentially stimulated by Wnt and frizzled homologs in a G-protein-dependent manner. *Current Biology* **9**:695–S1. doi: [10.1016/S0960-9822\(99\)80310-8](https://doi.org/10.1016/S0960-9822(99)80310-8), PMID: [10395542](https://pubmed.ncbi.nlm.nih.gov/10395542/)
- Sheldahl LC, Slusarski DC, Pandur P, Miller JR, Kühl M, Moon RT.** 2003. Dishevelled activates Ca2+ flux, PKC, and CamKII in vertebrate embryos. *The Journal of Cell Biology* **161**:769–777. doi: [10.1083/jcb.200211094](https://doi.org/10.1083/jcb.200211094), PMID: [12771126](https://pubmed.ncbi.nlm.nih.gov/12771126/)
- Slusarski DC, Corces VG, Moon RT.** 1997a. Interaction of Wnt and a frizzled homologue triggers G-protein-linked phosphatidylinositol signalling. *Nature* **390**:410–413. doi: [10.1038/37138](https://doi.org/10.1038/37138), PMID: [9389482](https://pubmed.ncbi.nlm.nih.gov/9389482/)
- Slusarski DC, Yang-Snyder J, Busa WB, Moon RT.** 1997b. Modulation of embryonic intracellular Ca2+ signaling by Wnt-5A. *Developmental Biology* **182**:114–120. doi: [10.1006/dbio.1996.8463](https://doi.org/10.1006/dbio.1996.8463), PMID: [9073455](https://pubmed.ncbi.nlm.nih.gov/9073455/)
- Slusarski DC, Pelegri F.** 2007. Calcium signaling in vertebrate embryonic patterning and morphogenesis. *Developmental Biology* **307**:1–13. doi: [10.1016/j.ydbio.2007.04.043](https://doi.org/10.1016/j.ydbio.2007.04.043), PMID: [17531967](https://pubmed.ncbi.nlm.nih.gov/17531967/)
- Tada M, Heisenberg CP.** 2012. Convergent extension: using collective cell migration and cell intercalation to shape embryos. *Development* **139**:3897–3904. doi: [10.1242/dev.073007](https://doi.org/10.1242/dev.073007), PMID: [23048180](https://pubmed.ncbi.nlm.nih.gov/23048180/)
- Thrasivoulou C, Millar M, Ahmed A.** 2013. Activation of intracellular calcium by multiple Wnt ligands and translocation of β-catenin into the nucleus: a convergent model of Wnt/Ca2+ and Wnt/β-catenin pathways. *Journal of Biological Chemistry* **288**:35651–35659. doi: [10.1074/jbc.M112.437913](https://doi.org/10.1074/jbc.M112.437913), PMID: [24158438](https://pubmed.ncbi.nlm.nih.gov/24158438/)
- Tóntson L, Babina A, Vösumaa T, Kopanchuk S, Rinken A.** 2012. Characterization of heterotrimeric nucleotide-depleted Gα(i)-proteins by Bodipy-FL-GTPγS fluorescence anisotropy. *Archives of Biochemistry and Biophysics* **524**:93–98. doi: [10.1016/j.abb.2012.05.017](https://doi.org/10.1016/j.abb.2012.05.017), PMID: [22659491](https://pubmed.ncbi.nlm.nih.gov/22659491/)
- Veeman MT, Axelrod JD, Moon RT.** 2003. A second canon. Functions and mechanisms of beta-catenin-independent wnt signaling. *Developmental Cell* **5**:367–377. doi: [10.1016/S1534-5807\(03\)00266-1](https://doi.org/10.1016/S1534-5807(03)00266-1), PMID: [12967557](https://pubmed.ncbi.nlm.nih.gov/12967557/)
- Vetter IR, Wittinghofer A.** 2001. The guanine nucleotide-binding switch in three dimensions. *Science* **294**:1299–1304. doi: [10.1126/science.1062023](https://doi.org/10.1126/science.1062023), PMID: [11701921](https://pubmed.ncbi.nlm.nih.gov/11701921/)
- Várnai P, Balla T.** 1998. Visualization of phosphoinositides that bind pleckstrin homology domains: calcium- and agonist-induced dynamic changes and relationship to myo-[3H]inositol-labeled phosphoinositide pools. *The Journal of Cell Biology* **143**:501–510. doi: [10.1083/jcb.143.2.501](https://doi.org/10.1083/jcb.143.2.501), PMID: [9786958](https://pubmed.ncbi.nlm.nih.gov/9786958/)

- Wallingford JB**, Fraser SE, Harland RM. 2002. Convergent extension: the molecular control of polarized cell movement during embryonic development. *Developmental Cell* **2**:695–706. doi: [10.1016/S1534-5807\(02\)00197-1](https://doi.org/10.1016/S1534-5807(02)00197-1), PMID: [12062082](https://pubmed.ncbi.nlm.nih.gov/12062082/)
- Webb MR**. 1992. A continuous spectrophotometric assay for inorganic phosphate and for measuring phosphate release kinetics in biological systems. *PNAS* **89**:4884–4887. doi: [10.1073/pnas.89.11.4884](https://doi.org/10.1073/pnas.89.11.4884), PMID: [1534409](https://pubmed.ncbi.nlm.nih.gov/1534409/)
- Webb SE**, Miller AL. 2003. Calcium signalling during embryonic development. *Nature Reviews Molecular Cell Biology* **4**:539–551. doi: [10.1038/nrm1149](https://doi.org/10.1038/nrm1149), PMID: [12838337](https://pubmed.ncbi.nlm.nih.gov/12838337/)
- Wiedemann C**, Cockcroft S. 1998. The role of phosphatidylinositol transfer proteins (PITPs) in intracellular signalling. *Trends in Endocrinology & Metabolism* **9**:324–328. doi: [10.1016/S1043-2760\(98\)00080-0](https://doi.org/10.1016/S1043-2760(98)00080-0), PMID: [18406297](https://pubmed.ncbi.nlm.nih.gov/18406297/)
- Wirtz KW**. 1991. Phospholipid transfer proteins. *Annual Review of Biochemistry* **60**:73–99. doi: [10.1146/annurev.bi.60.070191.000445](https://doi.org/10.1146/annurev.bi.60.070191.000445), PMID: [1883207](https://pubmed.ncbi.nlm.nih.gov/1883207/)
- Wodarz A**, Nusse R. 1998. Mechanisms of Wnt signaling in development. *Annual Review of Cell and Developmental Biology* **14**:59–88. doi: [10.1146/annurev.cellbio.14.1.59](https://doi.org/10.1146/annurev.cellbio.14.1.59), PMID: [9891778](https://pubmed.ncbi.nlm.nih.gov/9891778/)
- Wu D**, Jiang H, Katz A, Simon MI. 1993. Identification of critical regions on phospholipase C-beta 1 required for activation by G-proteins. *The Journal of Biological Chemistry* **268**:3704–3709. PMID: [8381437](https://pubmed.ncbi.nlm.nih.gov/8381437/)
- Xie Y**, Ding YQ, Hong Y, Feng Z, Navarre S, Xi CX, Zhu XJ, Wang CL, Ackerman SL, Kozlowski D, Mei L, Xiong WC. 2005. Phosphatidylinositol transfer protein-alpha in netrin-1-induced PLC signalling and neurite outgrowth. *Nature Cell Biology* **7**:1124–1132. doi: [10.1038/ncb1321](https://doi.org/10.1038/ncb1321), PMID: [16244667](https://pubmed.ncbi.nlm.nih.gov/16244667/)
- Ye X**, Ji C, Yin G, Tang R, Zeng L, Gu S, Ying K, Xie Y, Zhao RC, Mao Y. 2004. Characterization of a human Sec14-like protein cDNA SEC14L3 highly homologous to human SPF/TAP. *Molecular Biology Reports* **31**:59–63. doi: [10.1023/B:MOLE.0000013504.88003.32](https://doi.org/10.1023/B:MOLE.0000013504.88003.32), PMID: [15040456](https://pubmed.ncbi.nlm.nih.gov/15040456/)
- Zhang Y**, Li X, Qi J, Wang J, Liu X, Zhang H, Lin SC, Meng A. 2009. Rock2 controls TGFBeta signaling and inhibits mesoderm induction in zebrafish embryos. *Journal of Cell Science* **122**:2197–2207. doi: [10.1242/jcs.040659](https://doi.org/10.1242/jcs.040659), PMID: [19509062](https://pubmed.ncbi.nlm.nih.gov/19509062/)
- Zhang M**, Zhang J, Lin SC, Meng A. 2012. β -Catenin 1 and β -catenin 2 play similar and distinct roles in left-right asymmetric development of zebrafish embryos. *Development* **139**:2009–2019. doi: [10.1242/dev.074435](https://doi.org/10.1242/dev.074435), PMID: [22535411](https://pubmed.ncbi.nlm.nih.gov/22535411/)